Exciton dynamics and energy transfer processes in semiconductor nanocrystals

By

Andries Meijerink

Condensed Matter and Interfaces, Department of Chemistry, Debye Institute, Utrecht, The Netherlands

1. Introduction

Exciton dynamics provide unique information on both the nature of optical transitions and the local environment of an optically active species. However, experimental facilities for measuring (fast) luminescence decay dynamics have been developed long after techniques for time-averaged optical spectroscopy (absorption, excitation and emission spectroscopy). Studies on the dynamics of excited states therefore lag behind of steady state spectroscopy. This situation is also true for research on the optical properties of semiconductor nanocrystals. The first scientific record relating the change in optical properties of semiconductor nanocrystals to the particle size dates back to 1926 when Jaeckel explained the red-shift of the absorption onset in glasses containing CdS particles to a change in the CdS particle size [1]. It took until the 1980's that a fundamental understanding of the effects underlying the size-dependent optical properties of semiconductor nanocrystals were explained by quantum confinement and the name quantum dots (QDs) was introduced for these nanocrystals [2–4]. Since then the work on semiconductor nanocrystals has developed to an active and still growing field of research. Initially information on the optical properties of QDs was obtained from luminescence (excitation and emission) and absorption spectra. The results from the optical spectra could be related to theoretical calculations on the energy level structure. As for other optically active systems, additional information was later obtained from the dynamics of the excited state. The decay kinetics of the luminescence provide information on for example the nature of excited states, the quality of nanocrystals, competition between radiative and non-radiative recombination processes and interactions between QDs. At present, time resolved studies play a prominent role in the understanding of the optical properties of QDs. The time range involved varies between fs/ps (governed by non-radiative relaxation processes of charge carriers and energy transfer processes) to ns/μs (for radiative recombination processes).

The rapid increase in fast dynamics studies in the field of semiconductor nanocrystals, and in optical spectroscopy in general, has not only been triggered by the realization that decay kinetics provide important additional information on

their optical and electronic properties. It is also the spectacular development of experimentally available systems for fast (fs to ns) optical spectroscopy. Equipment for ps and ns lifetime measurements is now commonplace while even 20 years ago the building of a ps laser was a research project in its own. The development of ps diode lasers has resulted in cheap commercially available systems for sub-ns life time measurements, using time-correlated-single-photon counting techniques. For probing the faster dynamics of electron and hole relaxation processes within the conduction or valence band, Ti-sapphire fs laser-systems are available. In the past decade pump-probe systems for measuring fs carrier dynamics, for example by transient absorption spectroscopy, are becoming available in a growing number of laboratories. Alternatively, fast time-resolved emission spectra can be recorded on a ps time scale using a streak camera in combination with a Ti-sapphire laser.

In this chapter the exciton and charge carrier dynamics in quantum dots will be discussed with a focus of colloidal semiconductor nanocrystals. In the first part of this chapter, the recombination dynamics in isolated QDs will be considered. For different types of QDs the radiative and non-radiative relaxation processes are discussed in relation to theoretical work on energy level calculations and relaxation processes. The focus will be on the widely studied model systems CdSe and CdTe, but also results on other systems will be reviewed. The second part of this chapter is devoted to energy transfer processes between QDs. A short theoretical basis will be provided on energy transfer and energy migration after which exciton dynamics in a variety of QD systems will be treated. Again, the well-known model systems will be used to illustrate the state of the art of the knowledge on energy transfer processes in semiconductor nanocrystals. In addition to energy transfer between QDs, also energy transfer to other chromophores and to metal nanoparticles (NPs) will be covered since these processes are becoming increasingly important in many applications of QDs.

2. Exciton dynamics in quantum dots

2.1 General. The life time of the excitonic emission is an important parameter and contains information on the nature of the ground state and excited states of QDs. The theory for calculating the spontaneous emission probability for electric dipole transitions is well-established (Fermi's golden rule). The general equation for the transition probability between an excited state b and a ground state a is [5]:

$$A_{ba}(\mathrm{ED}) = \frac{1}{\tau_{\mathrm{rad}}} = \frac{1}{4\pi\varepsilon_0}\frac{4n\omega^3}{3\hbar c^3}\left(\frac{E_{\mathrm{loc}}}{E}\right)^2 \frac{1}{g_b}\sum_{a_n,b_m} |<a_n|\mu_c|b_m>|^2 \qquad (1)$$

where A_{ba} (ED) is the transition probability (s^{-1}) and is the inverse of the (radiative) life time τ_{rad}, n is the refractive index, ω is the transition frequency, $(E_{\mathrm{loc}}/E)^2$ is the local field correction factor and g_b is the degeneracy of the excited state. The summation is over all levels in the ground state a_n and excited state b_m for the transition dipole moments μ connecting the levels. For an allowed electric dipole transition the transition dipole moment $\mu = e{\cdot}r$ and with $r = 10^{-10}$ m (approximately

the Bohr radius of an hydrogen atom) and $n = 1.7$ this gives $A(\mathrm{ED}) = 10^8\,\mathrm{s}^{-1}$ in the visible spectral region. For QDs this equation is often rewritten as [6]:

$$A_{ba}(\mathrm{ED}) = \frac{2e^2\omega\varepsilon_1^{1/2}f}{3m_0c^3} \tag{2}$$

where the oscillator strength f is given by

$$f = \frac{2P^2}{m_0 E_{1\mathrm{S_h}1\mathrm{S_e}}}$$

P is the momentum transition moment of the exciton and is known as the Kane parameter. The expressions do not account for the screening of the electric field inside the QD. The high optical dielectric constants of semiconductors strongly influence the radiative lifetime. The internal electric field is reduced by dielectric screening and lengthens the life time by a factor $[3\varepsilon_0/(\varepsilon_1 + 2\varepsilon_0)]^{-2}$ where ε_1 is the (wavelength-dependent) dielectric constant of the semiconductor and ε_0 is the dielectric constant of the surrounding medium [6]. Semiconductor materials with large dielectric constants, like PbSe and PbS, have therefore long radiative life time.

In addition to radiative decay, non-radiative decay processes influence the decay kinetics of excitons in QDs. An important non-radiative relaxation process is trapping of an exciton or charge carriers at a defect or impurity site in the QD or at the QD surface. For measurements on an ensemble of QDs these non-radiative decay processes give rise to non-exponential decay curves. The distribution of defects or impurities over the QD population is inhomogeneous which results in a wide variety of (non-radiative) decay rates for different QDs in the ensemble. The exciton emission from QDs with a defect will decay faster with a total rate $A_{\mathrm{tot}} = A_{\mathrm{r}} + A_{\mathrm{nr}}$. The non-radiative decay rate A_{nr} will depend on the nature of the defect or impurity and the number of defects. QDs showing a single exponential decay are of high quality and exhibit a high luminescence quantum yield. For many studies it is crucial to use high quality QDs exhibiting a single exponential radiative decay. By studying the deviation of or changes in the single exponential decay, it will be possible to obtain quantitative information on for example energy transfer rates or factors influencing the radiative decay rate. If the reference decay curves are non-exponential due contributions from non-radiative decay processes, it is much harder to observe and analyze this influence. In addition to radiative and non-radiative recombination processes, also hot carrier relaxation and bi-exciton decay are interesting processes in exciton dynamics studies. One of the interesting topics in the past decades has been the question whether or not a phonon-bottleneck affects the exciton dynamics in QDs and more recently exciton dynamics studies have provided evidence for multiple exciton generation (MEG). In the sections below the various decay processes for different classes of QDs will be discussed.

2.2 Exciton dynamics in CdSe and CdTe quantum dots

2.2.1 *Radiative and non-radiative decay.* CdSe and CdTe nanocrystals are the most widely studied colloidal QDs and serve as the work horse for investigations

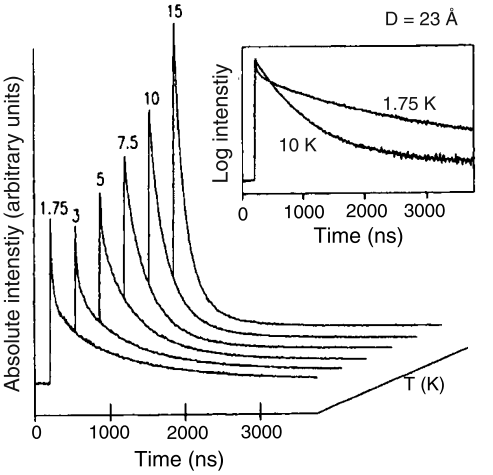

Fig. 1. Temperature-dependent decay curves for the exciton emission in 2.3 nm CdSe QDs. Reproduced with permission from [8], © 1994 APS

on quantum size effects. It is therefore not surprising that studies on the exciton dynamics have been done most extensively for CdSe and CdTe QDs and the understanding is the most advanced for these systems. First the exciton decay kinetics will be treated for CdSe QDs. Early studies on the exciton dynamics in CdSe QDs date back to 1994 shortly after the introduction of the hot-injection method for high quality CdSe nanocrystals [7]. Figure 1 shows the temperature-dependent decay profiles for 2.3 nm CdSe QDs. At the lowest temperatures a strongly non-exponential decay curve is observed with an initial decay in the ns range and long time decay in the μs range. Upon heating, the decay becomes single exponential (the short lived component disappears) and the long time component becomes faster and decreases from μs to ns between 2 and 15 K.

Later more extensive experiments and a theoretical analysis were applied to clarify the temperature-dependent decay behavior and relate the observations to the energy level scheme of CdSe QDs (wurtzite structure). Calculations show that the energy level structure is strongly dependent on the size and shape of the CdSe nanocrystal. In the effective mass approximation the $1S_e$ electron interacts with the $1S_{3/2}$ hole giving rise to an 8-fold degenerate state. The degeneracy is lifted by electron–hole exchange interaction, the crystal field and crystal shape asymmetry into five states which are denoted 0^L, 0^U, $\pm1^L$, $\pm1^U$ and ±2 [9]. The order of the states depends on the shape of the QD and the energy separation between the different states increases as the size of the QD decreases. The energy level structure of the $1S(e)–1S_{3/2}(h)$ is shown in Fig. 2, as it was calculated by Efros et al. [9]. Since then, more refined calculations and different models have been applied to explain the energy level structure but the main features are the same and are consistent with the experimentally observed temperature dependence of the decay time [10–12]. The transition from the lowest ±2 excited state of the CdSe QD to the ground state is formally forbidden. This results in a long lived emission at low temperatures. In addition, because of the low transition

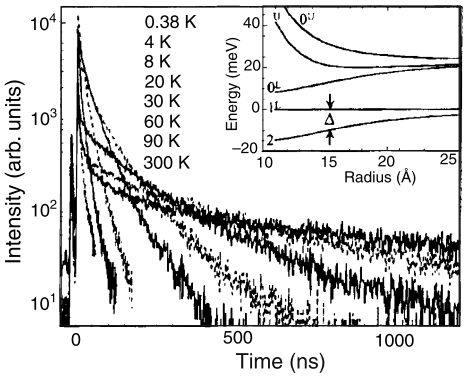

Fig. 2. Exciton emission decay curves for 2.6 nm core/shell CdSe/ZnS QDs between 0.38 K and 300 K. Inset shows results on theoretical calculations on the size-dependent energy level structure. Reproduced with permission from [14], © 2003 AIP

probability, transitions to this level cannot be observed in excitation or absorption spectra, so that this level has been named 'dark state'. Note however that the term 'dark state' is somewhat misleading since emission from this state at low temperatures can be very bright! Transitions from the $\pm 1^{L}$ level are allowed (this state is therefore called 'bright state') and at higher temperatures when the $\pm 1^{L}$ level is thermally occupied the exciton decay time drops from µs to ns. From the temperature dependence of the decay time the energy difference between the two lower excited states can be determined. The splitting is small, typically of the order of a meV.

A more careful analysis of the size and temperature dependence of the exciton life times for both ensemble of CdSe QDs (e.g. in [13, 14]) and single CdSe QDs [15] confirms the early observations. Figure 2 shows exciton decay measurements over a wide temperature range (0.38–300 K) for 1.3 nm CdSe QDs. Especially at the lowest temperatures, the very fast initial decay (ns) followed by a slow µs decay component can now be observed more clearly. Analysis of the results show that there is a size dependence of both the energy difference between the dark state and the bright state and the life time of the dark state. The energy difference and the dark state life time

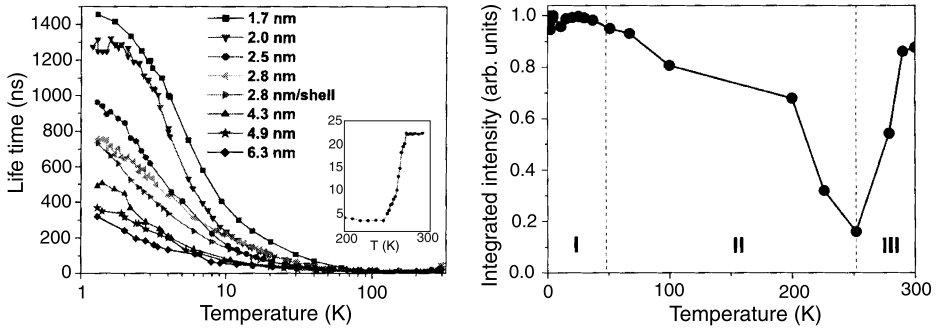

Fig. 3. (Left) Temperature dependence of the exciton emission life time for CdSe QDs between 1.7 nm and 6.3 nm, and (right) integrated emission intensity for CdSe QDs as a function of temperature. Reproduced with permission from [13], © 2006 APS

both increase for smaller particles. In Fig. 3 the temperature dependence of the long lived component of the excitonic emission is shown over a wide variety of CdSe QD sizes. In the low temperature regime the temperature dependence can be fitted fairly well to a three level model:

$$\frac{1}{\tau} = \frac{1}{\tau_{\text{dark}}}\left(\frac{e^{\Delta E/kT}}{1+e^{\Delta E/kT}}\right) + \frac{1}{\tau_{\text{bright}}}\left(\frac{e^{\Delta E/kT}}{1+e^{\Delta E/kT}}\right) \tag{3}$$

where τ_{dark} and τ_{bright} are the life times for the transition from the dark (± 2) and bright exciton state (± 1). Analysis of the size dependence shows that the splitting of the dark–bright state excitons increases from 0.7 meV to 1.7 meV upon decreasing the CdSe QD size from 6 nm to 1.5 nm [13]. The life time for the dark state decreases from 1.3 μs for the smallest particles to 0.3 μs for the largest (6 nm) CdSe QDs. In the literature there are various reports confirming this size dependence qualitatively although there are differences in the experimentally determined values in similar systems. Theoretical calculations on the size-dependent exciton splitting and life times, also confirm the observed trends as a function of particle size but usually give larger absolute values for the splitting and also the life times [9, 12]. The differences

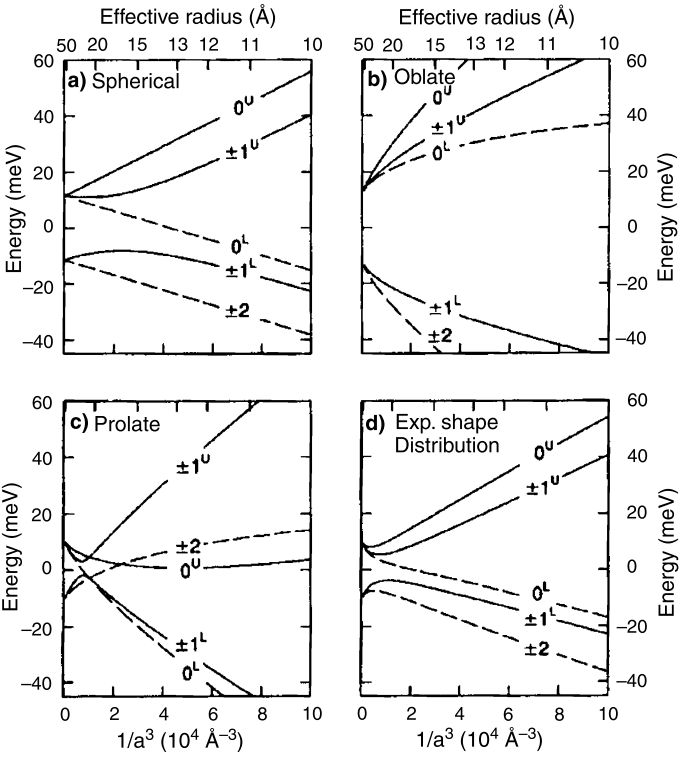

Fig. 4. Size dependence of the exciton band edge structure in CdSe QDs of various shapes. Solid lines represent states for which transitions to the ground state are allowed ('bright' states) while the dashed lines represent states for which transition to the ground state are formally forbidden ('dark states'). Reproduced with permission from [9], © 1998 APS

between observations and between observation and calculation are not surprising. Not only the size, but also the shape (and aspect ratio) of the QDs will strongly influence the energy level structure (see also Fig. 4). Small variations in shape for QDs of similar sizes can explain differences in the details. Also surface states have been suggested to strongly influence the energy level splitting and the life time of the dark state [9, 11, 12]. Interestingly, experiments on similar CdSe QDs with different cappings (organic ligands vs. ZnS) do not show a difference in the low-temperature decay behavior which suggests that the size-dependent and temperature-dependent exciton decay kinetics are intrinsic to the CdSe QDs and not caused by surface states.

At higher temperatures (above 50 K) temperature induced quenching of the exciton emission is observed. In Fig. 3, right hand side, this temperature region is labeled II. The quenching may be related to thermally activated trapping of charge carriers in surface states but the exact nature of the quenching process is not known. In this temperature region the decay curves become non-exponential which confirms that the shortening of the exciton decay time is not due to changes in the radiative decay rate but to quenching processes which have different rates for different QDs within the ensemble. The quenching behavior in this temperature regime is also dependent on the synthesis conditions. An interesting observation is the increase in life time in temperature region III. It is rather unusual that a luminescence decay time increases upon heating since most non-radiative decay processes becomes faster at higher temperatures. Not only the luminescence life time but also the luminescence intensity (quantum yield) increases around the transition temperature. This phenomenon has been called luminescence temperature anti-quenching and is explained by a phase transition in the capping layer [16]. At low temperatures the capping layer is 'frozen' and the rigid configuration of the surface capping molecules hinders relaxation of the Cd and Se surface atoms. It is well known that relaxation is required to prevent surface trapping states situated in the bandgap [12]. Upon 'melting' the surface capping layer, surface relaxation can occur and the disappearance of the surface quenching states causes an increase in the luminescence life time and luminescence intensity. Luminescence temperature anti-quenching has also been observed for CdTe QDs in ice. Here the quenching is related to local freezing of the solvent (water) around the CdTe QDs [17].

2.2.2 *Influence of the environment.* The discussion above beautifully illustrates an important aspect in research on QDs: the sensitivity of the luminescence properties of QDs to the surface. Subtle changes at the surface can strongly influence the luminescence properties and exciton dynamics of QDs. The surface to volume ratio is large and especially for the smaller QDs a significant fraction of the total number of atoms in the QDs is at surface sites. It is therefore no surprise that surface passivation is crucial. Synthesis procedures have been optimized to yield QDs with quantum yields close to unity and single exponential decay curves [18–20]. These highly efficient QDs are ideal probes to study the influence of the surroundings on the luminescence properties. Deviations from the exponential decay and changes in the luminescence life time can be related to changes in the environment. Here we will discuss two effects: the introduction of quenching molecules at the surface which causes non-radiative decay and changes in the refractive index or distribution of

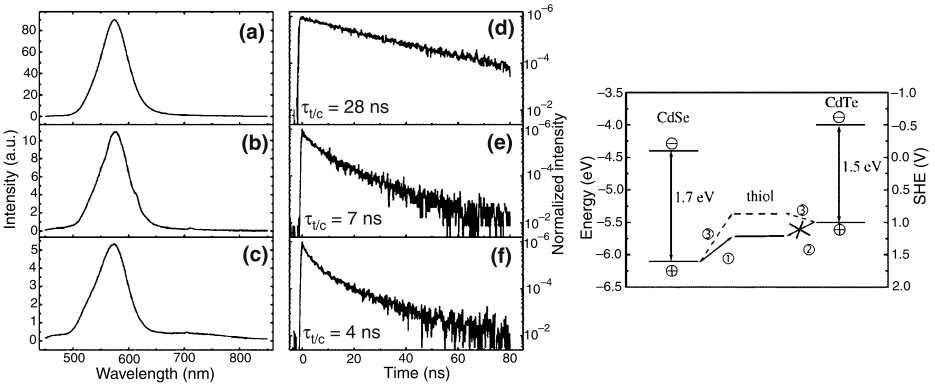

Fig. 5. (Left) Emission spectra and luminescence decay curves of the exciton emission of CdSe QDs capped with TOP/TOPO/HDA in chloroform (**a**, **d**), allylmercaptam in chloroform (**b**, **e**), and amino-ethane-thiol in water (**c**, **f**). (Right) Positions of bulk CdSe and bulk CdTe band edges with respect to a standard hydrogen electrode reference. Hole trapping can occur from CdSe (process ①) but not from CdTe (process ②). The dashed line indicates the assumed position for the standard potential of a thiol that quenches the luminescence of both CdSe and CdTe (process ③). Reproduced with permission from [21].

density of states in the surroundings of the QDs which influence the radiative life time.

As an example, Fig. 5 shows emission spectra and luminescence decay curves for CdSe QDs in chloroform [21]. Upon addition of allylmercaptam (Fig. 5B and E) or amino-ethane-thiol (Fig. 5C and F), quenching centers are introduced at the QD surface. As a result, the decay curves become non-exponential and show a faster decay ($\tau_{1/e}$ is 7 ns or 4 ns) while the emission spectra do not change. The single exponential decay curve in Fig. 5D shows that for this ensemble of QDs the decay is dominated by radiative relaxation. From the curve the radiative decay time (in this case 28 ns) can be determined. The quenching of the CdSe by thiols is related to trapping of holes in the valence band of CdSe by thiols (Fig. 5, right hand side). For CdTe the higher energy position of the valence inhibits this quenching and the luminescence life time of the CdTe emission remains single exponential with a $\tau_{1/e}$ of 17 ns [21].

A more subtle influence of the local environment is to change the radiative decay rate of the QD emission. Changing the nature of the surrounding medium (for example the solvent) causes a variation of the local field correction factor and this influences the radiative decay rate. In fact, QDs are a sensitive probe to test theoretical models on the influence of changes in the local surroundings on radiative decay processes. For CdSe and CdTe QDs it was shown that there is a weak but significant increase in the radiative decay rate in solvents with a higher refractive index [22]. For QDs in photonic bandgap structures the variation of the local density of states at specific wavelengths can be probed. The radiative decay rate was shown to be either enhanced or inhibited in line with a calculated increase or decrease of the density of states inside the photonic crystal [23]. In Fig. 6 on the left hand side an inverse opal of titania shells is shown which has a strong wavelength-dependent variation in the local density of states as a result of the periodic structure. On the right hand side the decay rates are plotted as a function of emission frequency (measured

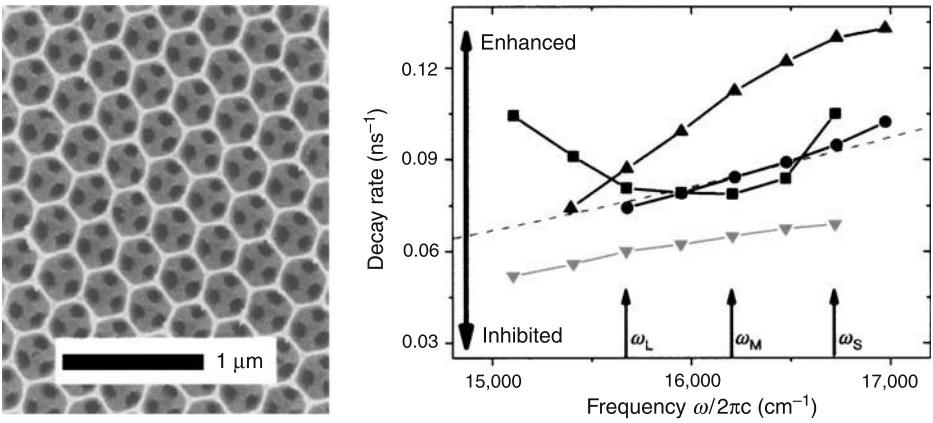

Fig. 6. (Left) Scanning electron microscope image of a (1 1 1) face of a titania inverse opal. (Right) Measured decay rates for CdSe/ZnSe QDs in photonic crystals with different lattice parameters (370 nm, filled dots; 420 nm, squares; 500 nm, upside-down triangles; 580 nm, triangles). The dashed curve gives the calculated decay rate in a homogeneous medium. Three sets of QDs (small, medium and large, central frequencies indicated by arrows) were used. Reproduced with permission from [23], © 2004 Nature

using a set of three size distributions of QDs in titania inverse opals). For example, in a photonic crystal with a lattice parameter of 580 nm a significant increase (up to a factor of 3) in the decay rate is measured and predicted in the energy range 16,000 cm^{-1} to 17,000 cm^{-1} due to the higher photonic density of states. Also note that the decay rate is not strongly influenced by the size of the QD. The dashed line in Fig. 6 gives the decay rate in a homogeneous medium (not photonic). There is an increase of the decay rate for the smaller sized QDs. The supra-linear increase has been explained by including variations in the thermal population over the various exciton states as a result of a size-dependent splitting of the energy levels [24].

2.2.3 *Fast relaxation processes.* A final aspect where carrier dynamics have received considerable attention is the relaxation of high-energy charge carriers to the band edges. In this process they loose their excess energy by interaction with phonons. The time scale of these relaxation processes is much faster than the time scale for the radiative and non-radiative recombination processes discussed above [25]. Typically these phonon relaxation processes take place in the 100 fs to 10 ps time regime. In bulk semiconductors typical rates are of the order of 0.5 eV/ps [26]. However, in a QD the discrete energy level structure and the change in the phonon spectrum can be expected to considerably reduce the phonon relaxation rates [27]. This phenomenon is known as the "phonon bottleneck". In the literature there are a number of beautiful demonstrations on how a phonon bottleneck can slow down the relaxation from a higher energy level, the most convincing experiments being on the work horse in solid state spectroscopy: ruby (Al_2O_3:Cr^{3+}) [28, 29]. The phonon bottleneck can even be used to create a "phonon laser" in ruby [29]. However, for semiconductor QDs contradictory results have been reported [30, 31]. In some papers reduced relaxation rates have been reported in QD structures (e.g. InGaAs

QDs) and ascribed to phonon bottleneck effects [25]. In CdSe and CdTe QDs the relaxation rates always show a fast ∼ps component while in some cases also a slower (∼100 ps) component has been observed and ascribed to a phonon bottleneck [25, 32]. The interest in a phonon bottleneck reducing the relaxation rate of hot charge carriers is not purely academic. If indeed the carrier relaxation is slowed down in QDs as compared to bulk semiconductors, this will be beneficial for the application of QDs in solar cells. Extraction of hot charge carriers (at a higher potential) gives the possibility of obtaining a higher voltage than the bandgap after absorption of high energy photons. A long life time of the hot charge carriers is required to make this feasible and this could be promoted by phonon bottleneck effects.

Most recent experiments on CdSe and CdTe indicate that there is no convincing evidence for a phonon bottleneck. This is not surprising. The justification for a phonon bottleneck is that the limited number of atoms in a semiconductor nanocrystal reduces the density of phonon modes. Since these are the accepting modes in the phonon relaxation process a reduced relaxation rate is plausible. However, the phonon density of states, especially in the higher energy region involved in the relaxation of hot charge carriers, is still sufficiently high to allow for fast relaxation while also coupling with high-energy vibrational modes in surface ligands contributes to fast charge carrier relaxation. There is however one exception: a phonon bottleneck does explain the slow relaxation process from the bright state to the dark state in CdSe QDs. These states are separated by a few cm^{-1}. At low temperatures (below 10 K) relaxation from the higher energy bright state to the lower energy dark is so slow that fast emission from the higher bright state is observed with a ns decay time (see Figs. 2 and 18). This shows that the relaxation from the bright $\pm 1^{L}$ state to the dark ± 2 dark state is slow (ns) which can be explained by the absence of accepting acoustic phonon modes that can bridge the meV gap between the two states. Due to the small size, the wavelength of the acoustic phonons is cut off, which effectively eliminates all low energy (∼meV) acoustic phonons [33].

To monitor the fast relaxation pump-probe techniques like transient absorption (TA) are very suitable. A fs pump pulse creates a hot electron–hole pair and subsequently a probe pulse can monitor the relaxation of the hot charge carriers to the band edges [34, 35]. By varying the photon energy (wavelength) of the pump pulse, the excess energy of the hot electrons and holes can be tuned. The absorption of a fs probe pulse is measured as a function of wavelength and time delay between the pump and probe pulse. The change in the absorption spectrum induced by the pump pulse is ascribed to two effects. First, the presence of the (hot) exciton influences the absorption due to Coulomb interactions of the electron–hole pair created by the pump pulse (which can also be considered as a shift in the absorption spectrum due to a Stark effect induced by the electron–hole pair). The second effect is the filling of states due to relaxation of the hot electrons and holes. For example, when the electrons have relaxed to the edge of the conduction band, absorption at wavelengths corresponding to transitions to the conduction band edge will be reduced due to the fact that the density of 'available' states is reduced (since the relaxed charge carriers occupy these states). In Fig. 7 an example of a transient absorption spectrum for 4.1 nm CdSe QDs is shown. From the transient absorption spectra at different delay times a wealth of information is obtained. For example, after an initial change in the

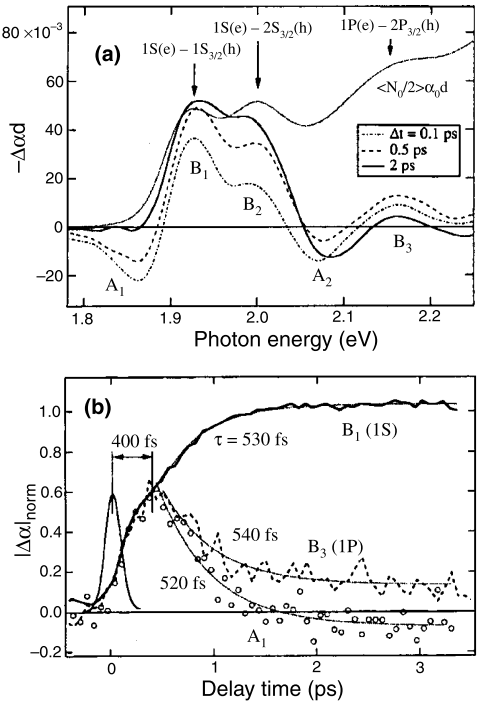

Fig. 7. **a** Transient absorption spectra of 4.1 nm CdSe QDs recorded with a 0.1 ps; 0.5 ps and 2 ps time delay, **b** Transient absorption kinetics at spectral position B_1 (thick solid line), B_3 (thick dashed line) and A_1 (circles). The thin solid line is the pump-probe cross-correlation profile. Reproduced with permission from [34], © 2000 ACS

absorption strength due to the Stark effect, it is observed that the absorption at the wavelength corresponding to B1 (absorption $1S(e)–1S_{3/2}(h)$) decreases with a time constant of 540 fs while the B3 absorption ($1P(e)–1P_{3/2}(h)$) increases with the same time constant. From this it can be concluded that the 1P–1S relaxation rate of conduction band electrons is about 540 fs. Further research has provided a fairly detailed understanding of the relaxation rates for different types of QDs and different sizes of QDs. Fast relaxation of electrons is mediated by energy transfer to holes (Auger process) which can relax through a large number of closely spaced energy levels in the valence band. The influence of the Auger cooling process is evident from experiments on QDs capped with molecules that efficiently trap holes (e.g. pyridine or thiols). A lengthening of the relaxation time from the sub-ps regime to several ps is observed when the holes are trapped thus blocking the Auger quenching process.

Further evidence for the fast intraband relaxation is obtained from single particle excitation spectra [36]. Experimentally it is very challenging to obtain a single particle excitation spectrum. The spectrum shown in Fig. 8 shows the energy level structure for a single CdSe QD. Even though the spectrum may seem to only contain information on the energy level structure, also information on relaxation rates can be obtained. The linewidth of excitation (and emission) lines of single particles reflect the homogeneous linewidth which is determined by the coherence life time of the

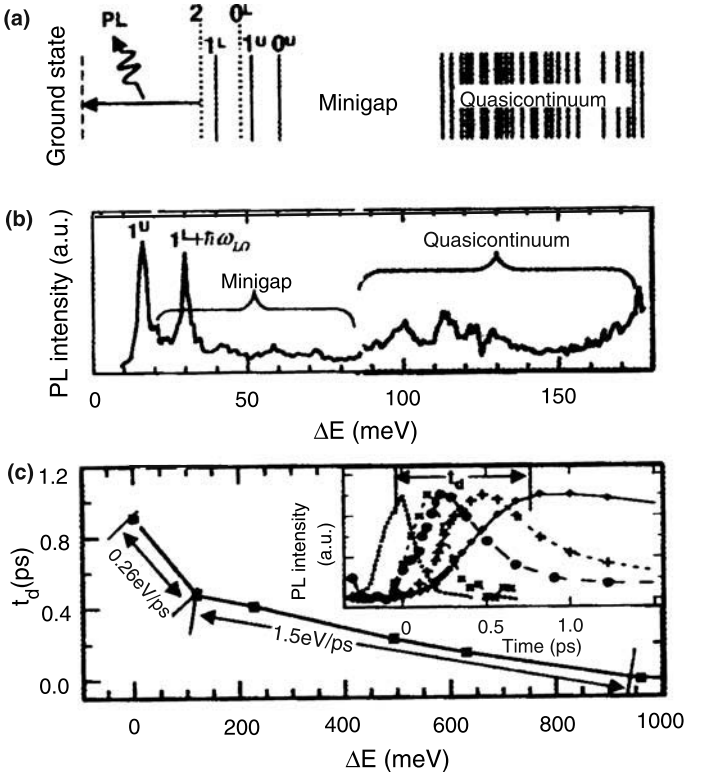

Fig. 8. **a** Schematic overview of the lower energy optical transitions in CdSe QDs, **b** single-QD excitation spectrum and **c** time delay of the hot photoluminescence maximum with respect to the arrival time of a pump pulse plotted as a function of the difference between detection energy and the energy of the lowest emitting transition (at 300 K). The relaxation rates are also indicated (in eV/ps). Reproduced with permission from [36], © 2004 APS

initial and final state through the Heisenberg uncertainty principle ($\Delta\nu = 5.3\ \mathrm{cm}^{-1}/\tau$ (ps)) [37]. The narrow excitation line corresponding to the 1^U transition indicates that the coherence lifetime for this excited state is relatively long, while the broader structures in quasicontinuum reflect fast relaxation from the states to the band edge states. The spectral width of $\sim 10\ \mathrm{cm}^{-1}$ is consistent with ps relaxation times.

The mechanism for the fast ps relaxation rate of hot electrons in QDs where Auger cooling has been suppressed by hole trapping shows that in this situation there is a strong influence of the vibrational modes of the capping molecules on the relaxation rate [26]. Figure 9 shows the 1P–1S relaxation profile for 5 nm CdSe QDs capped with different types of ligands. The relaxation time increases from 6 ps (in TOP/TOPO capped QDs) to 18 ps in *n*-dodecanethiol-capped QDs. The large variation in relaxation times is explained by energy transfer to resonant vibrational modes of the surface ligands. The faster relaxation rates are consistent with stronger surface ligand absorption peaks in the infrared region that is resonant with the 1P–1S transition.

Under high excitation powers the probability for the generation of multiple excitons in a single QD increases. The relaxation rate of these multi-exciton states

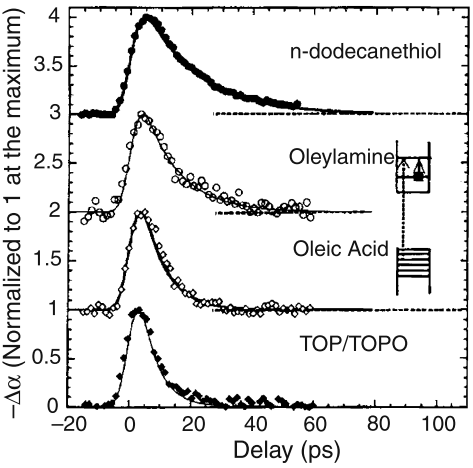

Fig. 9. Influence of capping molecules on the 1P–1S relaxation rate in CdSe QDs, measured by TA spectroscopy. Reproduced with permission from [26], © 2005 ACS

is extremely fast, again due to Auger quenching processes. The decay of the blue-shifted emissions takes place on a 100 ps timescale, the exact rate depends on the particle size (150 ps for 3.4 nm QDs and 50 ps for 2.3 nm QDs) [38, 39]. Also the radiative decay rate for bi-exciton and tri-excitons have been determined. Studies on the dynamics of the bi-excitons and tri-excitons in single CdSe core-shell QDs (5.1 nm) yielded values of 8.4 ns and 6.8 ns for radiative decay of bi-excitons and tri-excitons, respectively [39]. This is in line with theoretical predictions on the bi-exciton and tri-exciton decay.

2.3 Exciton dynamics in other types of quantum dots. Research on radiative and non-radiative relaxation processes in other QD systems is limited in comparison to the widely studied CdSe and CdTe model systems discussed above, although there is rapid increase in research on carrier dynamics in IV–VI PbSe and PbS QDs. These infrared emitting QDs have gained considerable interest since reports on efficient multiple exciton generation MEG upon excitation with photons exceeding 2.5 E_g [40, 41]. Hot carrier relaxation plays an important role in explaining the high efficiency of this process since it is competing with MEG. The radiative life time of the emission from PbSe and PbS QDs is long, typically in the μs regime [6, 42–44]. As an example a decay curve of PbSe QD emission is shown in Fig. 10 together with the absorption and emission spectra for these nanocrystals [6]. The quantum yield can be high (up to 85%) and the decay curve shown in the inset represents the radiative decay of these QDs. The luminescence decay time of 0.88 μs is considerably longer than the ns decay times observed for CdSe or CdTe QDs. Similarly long luminescence life times are reported for PbS QDs. The origin for the long life time is explained by dielectric screening as discussed above and is in good agreement with theoretical calculations [6, 44].

An interesting question is whether or not a lengthening of the radiative decay time will occur upon cooling. The most recent theoretical calculations predict a dark state

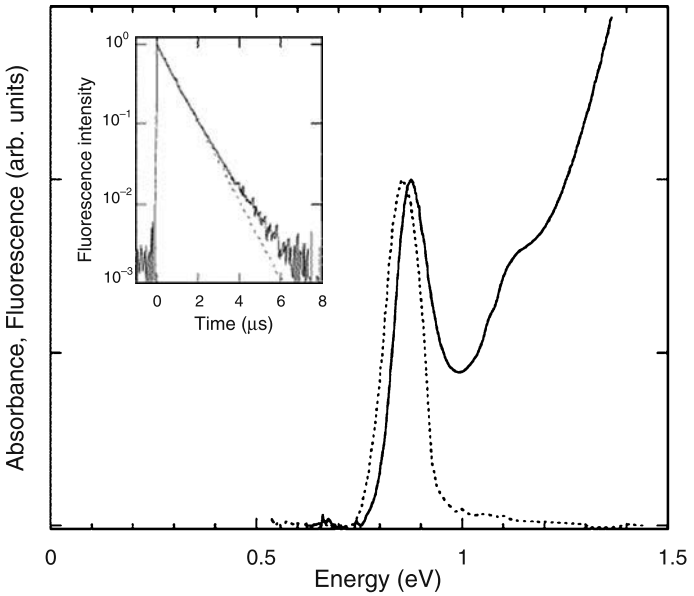

Fig. 10. Emission (dotted line) and absorption (drawn) spectrum of PbSe QDs. The inset shows the luminescence decay curve. Reproduced with permission from [6], © 2002 ACS

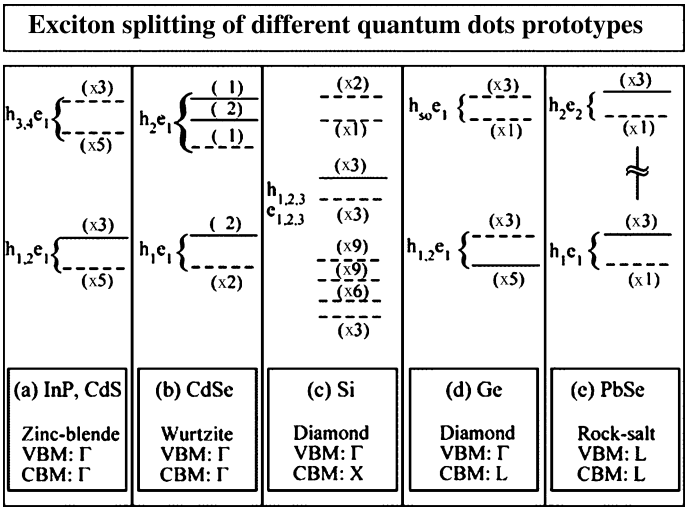

Fig. 11. Energy level diagram of the splitting of the lowest exciton state from pseudopotential calculations. Solid lines represent bright states (allowed transition to the ground state) and broken lines represent dark states (forbidden transitions). Reproduced with permission from [44], © 2007 ACS

to be lowest energy exciton state in PbSe QDs (see Fig. 11). Just as for CdSe and CdTe QDs this is expected to result in a long decay time upon cooling. At this point, no experimental results have been published on the temperature dependence of the life time of the exciton emission in PbS or PbSe QDs. Initial (unpublished) results do not

provide evidence for substantial lengthening of the decay time at temperatures down to 4 K suggesting that either the lowest exciton state is not a dark state or the splitting between the dark and bright state is much smaller than 1 meV [45].

A beautiful illustration of how the measurement of the dynamics of excitons can be used is the recent observation of multiple exciton generation in PbS and PbSe QDs. Upon excitation of these IV–VI QDs with photons of energies exceeding $\sim 2.5\ E_g$ multiple excitons are generated in a single QD [40, 41]. The fingerprint for multiple exciton generation is the observation of fast decaying components in the transient absorption spectra resonant with the $1S(e)–1S_{3/2}(h)$ transition: only when bi-excitons are created, a fast filling of these band-edge states is expected (for a single exciton state the time constant for filling is the (ns) single exciton decay rate). From the ratio of the TA signal for the single exciton decay and the fast component, the number of excitons generated after absorption of a single high-energy photon can be estimated. Analysis of the results shown in Fig. 12 indicates that the efficiency of multiple exciton generation is surprisingly high (700% for photons of 8 E_g). The mechanism responsible for MEG is unclear but, if the reported efficiencies for MEG are correct, it must take place on a fs time scale. To explain the high efficiency the creation of

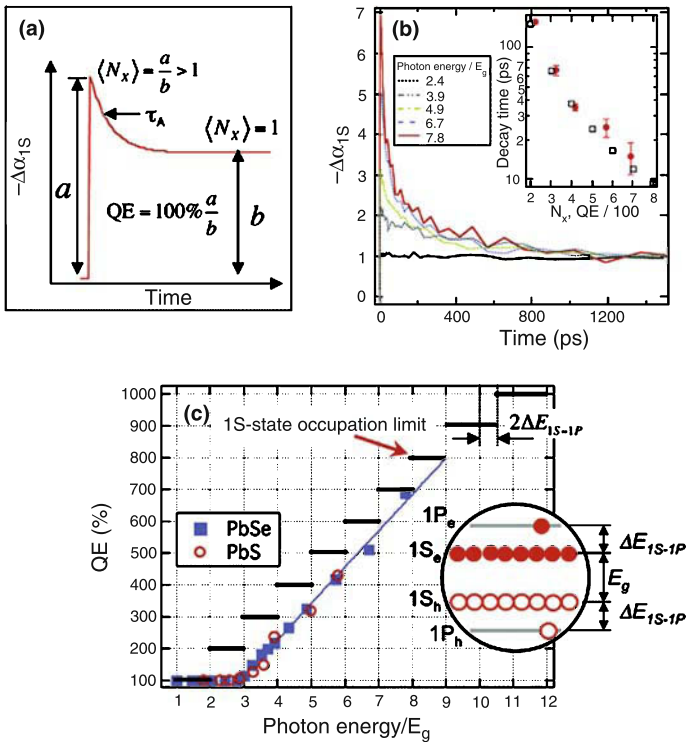

Fig. 12. **a** Schematic picture of the method to derive MEG yields from the transient absorption (TA) curve. **b** Experimentally measured transient absorption at the band edge transition after (low power) excitation with various photon energies (indicated in the figure). **c** Efficiency of exciton generation (number of excitons per absorbed photon)

multiple excitons has to occur much faster than competing processes (like hot carrier relaxation) which take place on a ps time scale.

After the observations of MEG in PbS and PbSe, reports appeared on MEG in other systems like CdSe, InP and Si QDs [46–48]. However, later the claim for MEG in InP QDs was withdrawn while for CdSe QDs contradictory results were reported for seemingly the same experiment. The difference in the results are possibly related to a trivial aspect as stirring (no MEG) or not stirring (MEG) the QD solution [49]. The controversy shows that fast dynamic measurements do not only provide a wealth of information, but are at the same time extremely sensitive for several external parameters and the interpretation is not always straightforward.

For III–V QDs extensive research has been done on exciton dynamics in epitaxially grown QD structures. For I–VII QDs like CuCl exciton dynamics have also been extensively studied. This chapter focuses on colloidal QD systems and the reader is referred to [50] and [51] for further information on exciton dynamics in III–V and I–VII QD structures. InP is an exception since these III–V QDs have been widely studied as colloidal nanocrystals. The radiative life time of the exciton emission is similar to that of CdSe and CdTe QDs. For efficient red-emitting InP QDs a decay time of 65 ns has been reported at room temperature [52]. The II–VI ZnO QDs are also widely studied, but the radiative life time of the exciton emission is hard to determine since trapping of charge carriers in defects occurs (giving rise to the well-known green emission from ZnO) and hinders the observation of the radiative decay rate. From the multitude of studies on ZnO nanostructures it is clear that exciton relaxation is fast and typically sub-ns life times are observed, even in systems where trapping of charge carriers is prevented by trap filling [53, 54]. These results suggest that the radiative rate for the exciton emission in ZnO is an order of magnitude faster than in CdSe and CdTe QDs. Finally, an important class of QDs are Si and Ge QDs. For Si nanocrystals the discussion on the nature of the blue-shifted emission has been long debated (and the debate is still going on) [55, 56]. From many studies it is however clear that Si nanocrystals can show blue-shifted emission due to quantum confinement. The life of the emission is long, μs-ms and is related to the forbidden nature of the indirect bandgap transition [57, 58].

3. Energy transfer processes with quantum dots

3.1 Energy transfer and energy migration. In diluted systems the optical properties and time response are determined by the properties of the single (isolated) QD. When the concentration of QD is increased or when clusters of QDs are formed, energy transfer between QDs in close proximity becomes an important alternative pathway for de-excitation of a QD. Energy transfer between optically active ions and molecules is well known [5]. The initially excited species is called the donor and the excitation energy can be transferred from a donor to an acceptor in close proximity. In the case of QDs energy transfer will be directed from the smaller QDs (higher energy bandgap) to the larger QDs (smaller energy bandgap).

Quantitative modeling and understanding of energy transfer processes between luminescent ions and molecules has greatly benefited from the work by Förster and Dexter in the 1950's. Equations were derived for energy transfer rates for various

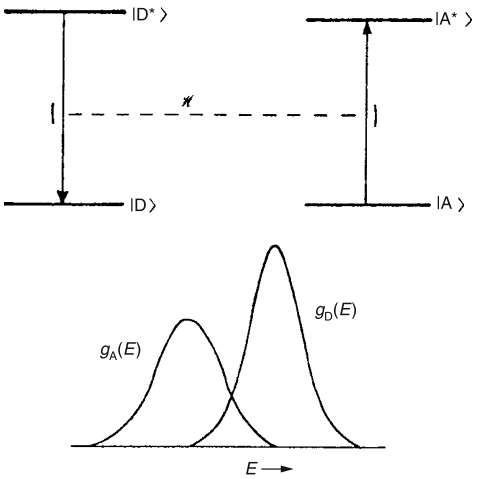

Fig. 13. Schematic representation of energy transfer from a donor D to an acceptor A. Both interaction (top picture) and spectral overlap (bottom picture) are required. Reproduced with permission from [5], © 1989 Oxford University Press

mechanisms, i.e. multipole–multipole interaction and exchange interaction. In both cases energy transfer does not involve the emission of a photon. It concerns non-radiative energy transfer where the energy transfer is mediated by electrostatic coupling, magnetic coupling or exchange coupling between donor and acceptor. The concept is schematically depicted in Fig. 13. The general expression for the probability of energy transfer is given by [5]:

$$W_{\mathrm{DA}} = \frac{2\pi}{\hbar} |<\mathrm{D}, \mathrm{A}^*|H'|\mathrm{D}^*, \mathrm{A}>|^2 \int g_{\mathrm{D}}(E) g_{\mathrm{A}}(E) \mathrm{d}E \tag{4}$$

Here the left hand side represents the interaction between the donor and acceptor ion involved in the energy transfer process (multipole–multipole or exchange) and the right hand side term gives the overlap integral between the donor emission spectrum and the acceptor absorption spectrum (resonance condition). In the case of dipole–dipole interaction (the dominant mechanism for energy transfer in most cases discussed here) the equation becomes [5]:

$$W_{\mathrm{DA}}^{\mathrm{dd}} = \left(\frac{1}{4\pi\varepsilon_0}\right)^2 \frac{3\pi\hbar e^4}{n^4 m^2 \omega^2} \frac{1}{R^6} f_{\mathrm{D}}(\mathrm{ED}) f_{\mathrm{A}}(\mathrm{ED}) \int g_{\mathrm{D}}(E) g_{\mathrm{A}}(E) \mathrm{d}E \tag{5}$$

where $W_{\mathrm{DA}}^{\mathrm{dd}}$ is the energy transfer rate (through dipole–dipole interaction), R is the distance between the (point) dipoles, f_{A} and f_{D} give the (electric dipole) oscillator strengths for the acceptor and donor transition, the integral is the spectral overlap while the other symbols have their usual meaning.

Often the Förster equation is rewritten to give the energy transfer rate k [5]:

$$k_{\mathrm{Förster}} = \frac{Q_{\mathrm{D}}}{\tau_{\mathrm{D}}} \left(\frac{8.785 \times 10^{-25} I}{n^4 R^6}\right) \quad \text{with } I = \int_0^\infty \alpha_{\mathrm{A}}(\lambda) f_{\mathrm{D}}(\lambda) \lambda^4 \mathrm{d}\lambda \tag{6}$$

where Q_D is the dipole moment of the donor transition, τ_D is emission life time, R is the distance between the dipoles and I is overlap integral over acceptor extinction coefficient (α_A) and the donor oscillator strength (f_D) over the full wavelength interval. An interesting question concerns the validity of the (widely applied) Förster model to quantitatively describe energy transfer between QDs. The Förster model has been derived for the limit of point dipoles (i.e. the distance between the dipoles is much larger than the spatial extension of the dipoles). In the case of energy transfer between QDs this boundary condition is not valid. The oscillating dipoles in the QDs cannot be considered as point dipoles and also local fields can play an important role. In general the transfer rates calculated using the Förster equation are nevertheless in good agreement with the observed rates. In a recent theoretical paper on the validity of Försters theory for energy transfer between QDs it was concluded that Förster theory cannot be applied for energy transfer between indirect bandgap semiconductor nanocrystals like Si [59].

In Fig. 14 the luminescence decay profiles are sketched for different types of energy transfer processes [5]. In the absence of energy transfer processes (curve a), a single exponential decay is observed and the decay rate (radiative and non-radiative) can be determined from the emission life time. In the case of one-step energy transfer (curve b), the excitation energy is transferred from a donor to one or more acceptors in the immediate surroundings but there is no energy transfer between donors. In the luminescence decay curves this leads to an initial non-exponential decay that is faster than the radiative decay rate. The faster non-exponential decay reflects the different acceptor configurations around the donor. In the long time regime the decay time approaches the radiative decay rate for those donors that do not have an acceptor in the immediate surroundings. In case of concentrated systems of donors, energy

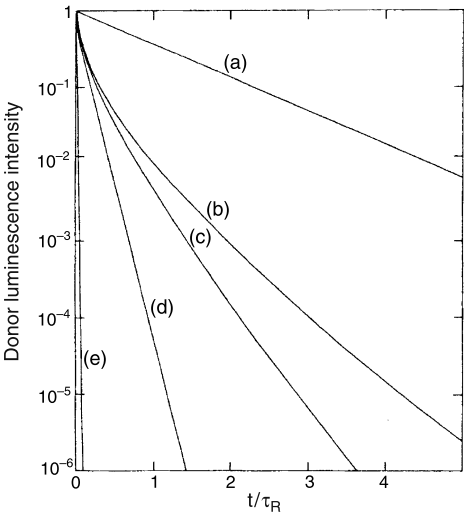

Fig. 14. Shape of luminescence decay curves of the donor emission for **a** isolated donors, **b** single step energy transfer to acceptors, **c** diffusion limited energy migration to acceptors and **d** and **e** fast diffusion. Reproduced with permission from [5], © 1989 Oxford University Press

transfer between donors can occur and energy transfer to acceptors or quenching sites can occur via diffusion of the excitation energy over the donor sublattice. If the energy transfer probability between donors is lower than the transfer probability to the traps, one speaks of diffusion limited energy migration and the luminescence decay is non-exponential (curve c). The initial fast non-exponential component reflects the single step energy transfer from donors to nearby acceptors (just as in curve b) but in the long time regime the decay is faster than the single exponential decay for isolated donors due to energy migration over the donor sublattice to acceptors, thus providing an additional decay channel. Finally, there is the regime of fast diffusion where the donor–donor transfer rate is much higher than the donor–acceptor transfer rate. In this case, a single exponential decay is observed (curves d and e) since all donors sense the same environment of acceptors due to the very rapid diffusion of the excitation energy over the donor sublattice.

The theory for analysis of the donor emission decay profiles and extracting information for donor–donor and donor–acceptor transfer rates is extensive in the literature on luminescence of transition metal ions and fluorescent molecules. In the case of random distributions of optically active species (glass like systems) decay profiles are fitted using the Inokuti–Hirayama model (for single step D–A energy transfer) and the Yokoto–Tanimoto model (in case of diffusion limited energy migration). For crystalline systems where energy transfer is dominated by short range energy transfer, the better models are shell models where the actual (discrete) distribution of acceptors is modeled based on the discrete donor–acceptor distances that are possible in the given crystal structure [60, 61].

3.2 Energy transfer between quantum dots. In the field of energy transfer processes involving QDs the analysis is more complicated and often more phenomological models are used to describe the observed decay behavior. An important difference between energy transfer processes between transition metal ions or fluorescent molecules and QDs is the homogeneity of the system. The inhomogeneous broadening for optical transitions is larger for QDs, usually much larger than the homogeneous broadening. This gives rise to a variable energy mismatch for energy transfer processes between QDs and it is hard to derive a single transfer rate for QDs at a certain distance. The energy mismatch needs to be made up by phonon assistance and the energy transfer probability for a given donor–acceptor pair at the same distance R will vary due to differences in the energy mismatch. This gives rise to a distribution in the donor–acceptor transfer rates. A second aspect is the inhomogeneity in the distribution of distances between QDs. There is a wide variety of systems where energy transfer between QDs has been studied, as will be discussed below, but rarely one can determine the distribution in distances between donors and acceptors with the same accuracy as it can be done for transition metal ion-doped crystals where the crystal structure imposes discrete donor–acceptor distances. Only in well-ordered self-assembled structures of QDs one can obtain more quantitative information on the number of acceptors at specific distances. In spite of the more complex nature of energy transfer processes in QD systems, it is useful to be aware of the analysis methods developed for energy transfer processes between optically active transition metal ions since they can serve as a starting point for the analysis.

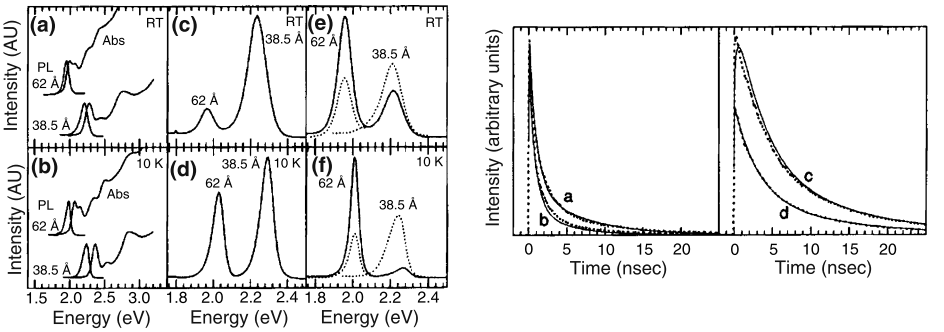

Fig. 15. (Left) Absorption and emission spectra for a mixture of 3.9 nm and 6.2 nm CdSe QDs at RT **a** and 10 K **b**. In **c** and **d** the photoluminescence spectra for a (frozen in (d)) solution with 18% 6.2 nm (acceptor) and 82% 3.9 nm (donor) QDs are shown at RT and 10 K. In **e** and **f** the RT and 10 K emission spectra of close packed solid films are shown. (Right) Luminescence decay curves of the emission from the 3.9 nm QDs in a pure film of 3.9 nm QDs (a) and a mixed film with 18% of 6.2 nm QDs (b). Curves (c) and (d) show the decay curves of the emission from the 6.2 nm QDs in the same mixed film upon excitation in blue (c) and red (d) absorption edge of the 3.9 nm CdSe QDs. Reproduced with permission from [62], © 1996 APS

In two pioneering papers on energy transfer between QDs, Kagan et al. studied the energy transfer from small 3.9 nm CdSe QDs to large 6.2 nm CdSe QDs in thin solid films of QDs with 18% of the large QDs and 82% of the smaller (donor) QDs [62, 63]. Spectroscopic evidence for the presence of efficient energy transfer from the smaller to the larger QDs is provided by comparison of Fig. 15c and d to e and f: the 2.3 eV emission from the smaller QDs is clearly quenched in the solid films. The luminescence decay curves were analyzed using a model similar to the Inokuti–Hirayama model:

$$n_{\mathrm{D,mixed}}(t) = n_{\mathrm{D,pure}}(t)\exp\left[-\gamma\left(\frac{\pi t}{\tau_{\mathrm{D}}}\right)^{1/2}\right] \tag{7}$$

where $\gamma = C(4/3\pi R_0^3)$. From the fit (drawn line for the right hand side of Fig. 15, curve (a)) the critical distance for energy transfer was determined to be 4.8 nm and was found to be in agreement with the critical distance for energy transfer derived using the Förster equation.

This gives a nearest neighbor transfer rate of $1\times10^8\,\mathrm{s}^{-1}$ at RT and $0.6\times10^8\,\mathrm{s}^{-1}$ at 10 K. The nearest neighbor distance between can be estimated as 6.1 nm (the sum of the radii of the QDs (5 nm) and the thickness of the capping layer (1.1 nm)). This value for the nearest neighbor separation distance was confirmed by SAXS measurements. Finally, the nearest neighbor energy transfer rates were also determined using the Förster equation for dipole–dipole interaction and found to be an excellent agreement with the experimentally determined values showing that dipole–dipole interaction is the dominant mechanism for energy transfer between nearest neighbor QDs.

In addition to the model resembling the Inokuti–Hirayama model, also more exact shell models have been applied, in analogy with the analysis of energy transfer between luminescent ions in solids [64]. Langmuir–Blodgett (LB) assemblies of

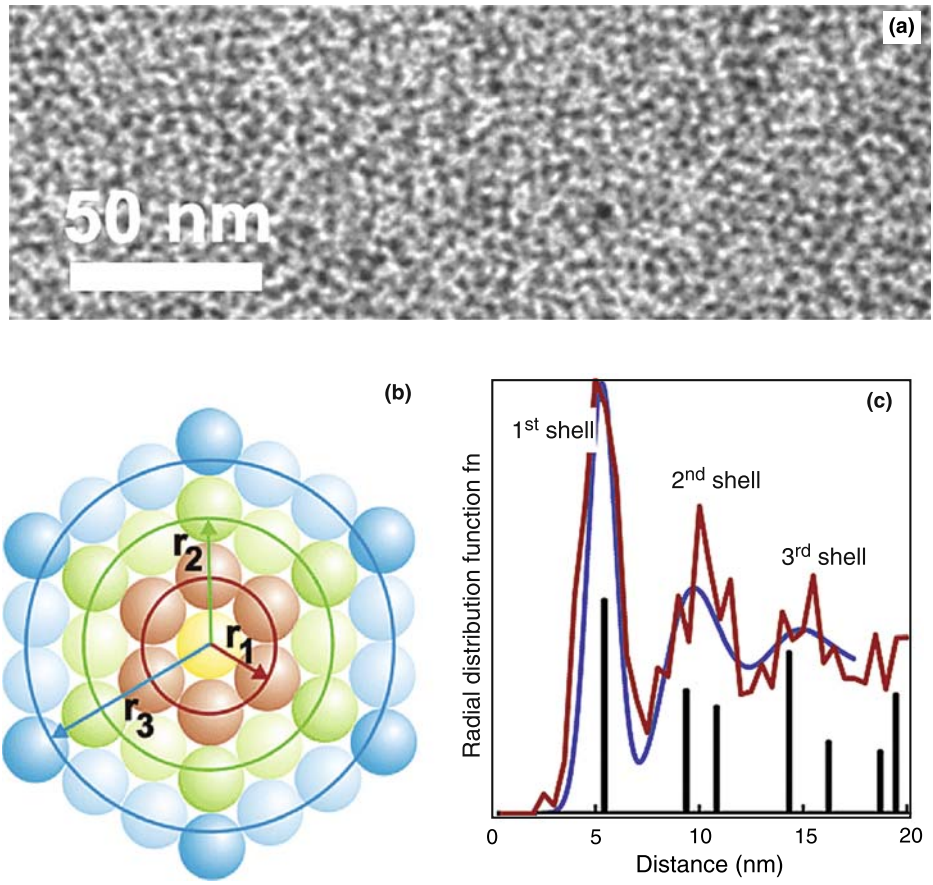

Fig. 16. **a** A TEM image of an LB monolayer of octylamine-capped CdSe NQDs with radius $R = 2.2$ nm. **b** An ideal hexagonal 2D array of spheres. Different colors show three main shells. Different shadings within the main shells show different subshells. **c** Radial distribution function (RDF) of the LB sample shown in panel a (red line). Black bars represent the RDF of an ideal hexagonal array composed of spheres with a center-to-center distance of 5.4 nm. The blue line is the RDF of a "non-ideal" hexagonal array with fluctuation in the sphere-to-sphere distances of 13%. Reproduced with permission from [64], © 2003 ACS

octylamine-capped 2.2 nm CdSe QDs were prepared and the luminescence decay curves were analyzed at different wavelengths within the inhomogeneously broadened line. In Fig.16a TEM image of the Langmuir–Blodget film is shown, together with the distribution of donor–acceptor distances within this ordered film (Fig. 16c). For this situation the luminescence decay curves can be modeled for different wavelengths within the inhomogeneously broadened line. The nearest neighbor transfer time was determined to be 50 ps, yielding transfer times of 0.75 ns and 10 ns for transfer to acceptors in the 2nd and 3rd shell. A good agreement between the experimentally determined transfer rates at different emission energies was obtained using these three rates and statistical determinations of the number of acceptors in each shell as a function of emission energy. The transfer time of 50 ps is considered to

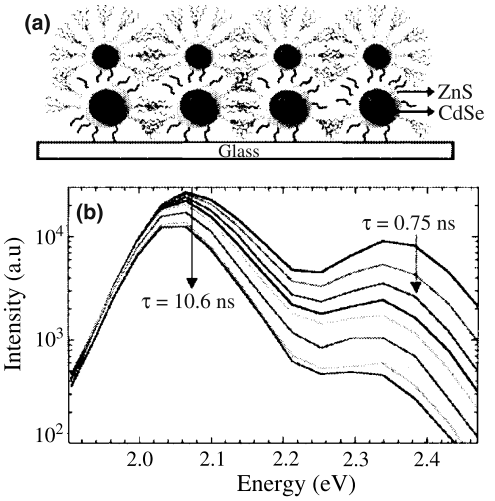

Fig. 17. (Top) Schematic picture of a QD bilayer in which directional energy flow from the smaller to larger QDs can occur. (Bottom) Time-resolved photoluminescence spectra recorded with 500 ps time intervals. Reproduced with permission from [66], © 2002 APS

represent an upper limit for the transfer rate that can be expected for energy transfer between CdSe QDs.

Energy transfer between QDs of different sizes is not only of scientific interest, it may also be applied for light harvesting purposes. By constructing layered structures of QDs where the size of the particles is decreased or increased in every subsequent layer, a system in which a directional flow of energy occurs to the layer with the largest QDs [65, 66]. In this way all the excitation energy that is absorbed by a large number of QD layers can be concentrated in a single layer. To demonstrate the efficiency of this light harvesting concept, directional energy transfer in a bi-layer is demonstrated in Fig. 17. A bilayer of 1.3 nm on top of 2.1 nm core-shell CdSe/ZnS QDs was fabricated. The lower part of Fig. 17 shows emission spectra at 500 ps time interval. The emission from the smaller QDs decay with a time constant of 750 ps due to fast energy transfer to the larger dots which decay with a time of 10.6 ns, close to the radiative decay time. The large ratio (20) between the interlayer transfer rate and the radiative decay rate allows for efficient transfer up to 20 layers of QDs of continuously increasing sizes.

Evidence that the mechanism for the energy transfer process is dipole–dipole (or in general: multipole–multipole) interaction is demonstrated by studying the temperature dependence of the energy transfer rate and the efficiency of the energy transfer process [67]. In the case of dipole–dipole interaction, the energy transfer rate is proportional to the oscillator strengths of the transitions involved on the donor and acceptor. Since both the transfer rate and the radiative decay of the donor are proportional to the oscillator strength of the transition on the donor, the transfer efficiency (or the ratio of the donor/acceptor emission intensity) is expected to be independent on the oscillator strength of the transition on the donor. In the case of CdSe or CdTe QDs the oscillator strength of the donor transition can be easily tuned

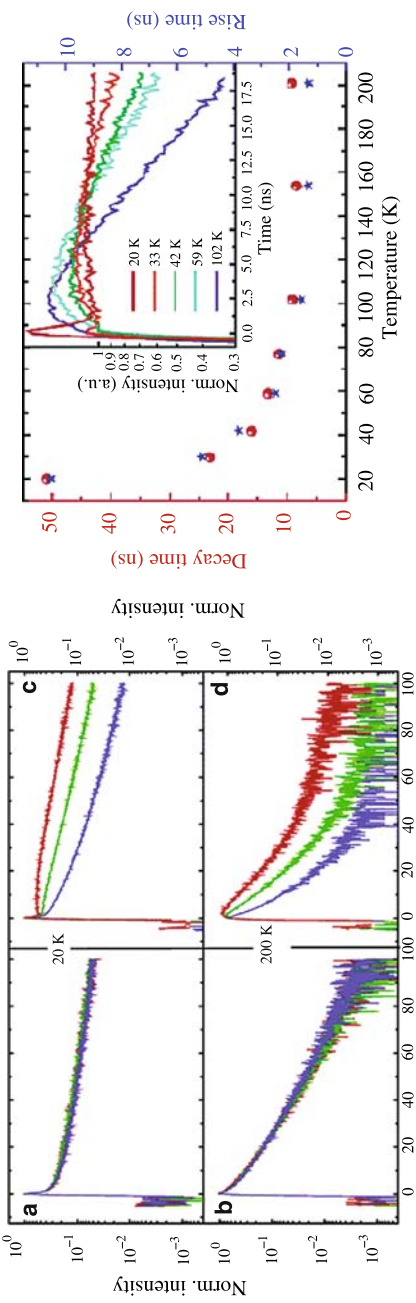

Fig. 18. (Left) Normalized luminescence decay curves of orange emitting CdTe QDs dissolved in chloroform (**a**, **b**) and as a QD solid on quartz (**c**, **d**) at 20 K and 200 K measured at the peak maximum (green) 20 nm red-shifted (red) and 20 nm blue-shifted (blue) from the maximum. (Right) Luminescence decay (●) and rise time (★) of a QD solid on quartz, prepared from orange-luminescing hexanethiol-capped CdTe QDs recorded as function of temperature, measured 20 nm red-shifted of the excitonic peak maximum. The inset shows an enlargement of the normalized luminescence decay curves at different temperatures in the first 18 ns. Note the fast component at low temperatures which is due to emission from the bright state. Reproduced with permission from [67], © 2005 ACS

by cooling the QDs and freezing the system partly in the dark state. The spectral shift involved is small and will not influence the transitions involved on the (larger) acceptor QDs. In Fig. 18 results on temperature dependence of the donor emission decay curves is shown for orange emitting CdTe QDs (3 nm) in chloroform at low concentration (no energy transfer expected) and as a QD solid on quartz (energy transfer possible). Decay curves were recorded as a function of temperature in the maximum and on the short wavelength side and long wavelength side of the inhomogeneously broadened emission band. From the faster decay curves in the solid for the short wavelength side (donors) and the rise time on the long wavelength side (acceptors) the energy transfer rate can be determined. The decay curves in the solvent (no energy transfer) serve as a reference. The results in Fig. 18b show that the energy transfer rate is proportional to the radiative decay rate on the donor, consistent with a dipole–dipole energy transfer mechanism. Further evidence was obtained from the temperature dependence of the transfer rate in mixed solids of green (donor) and orange (acceptor) QDs systems. Also in this system the transfer rates are observed to scale with donor emission decay rate while the transfer efficiency is not influenced by the temperature.

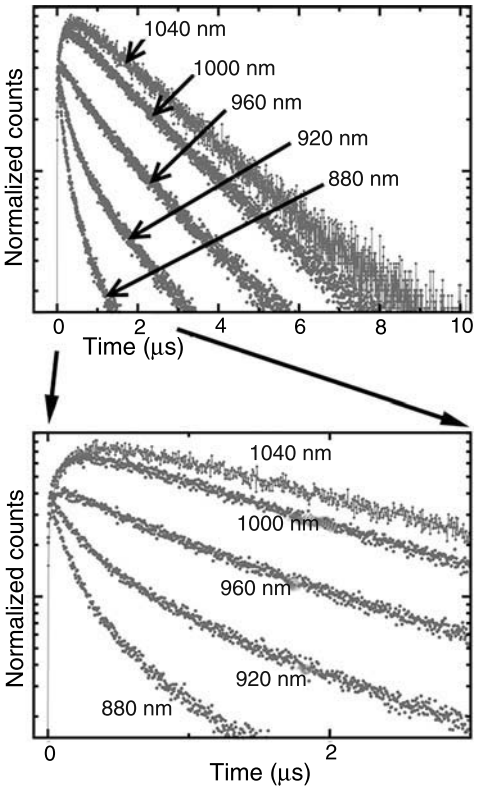

Fig. 19. Temporally resolved fluorescence of a film of 2.5 nm PbS QDs at different wavelengths within the emission band for the 0–10 μs window (top) and the 0–3 μs window (bottom) at RT. Reproduced with permission from [43], © 2007 ACS

Similar conclusions are obtained by studying energy transfer processes in PbS QD solids [43]. The RT radiative decay time of the PbS exciton emission is of the order of 1 μs, about two orders of magnitude slower than the ~20 ns decay time of the CdSe or CdTe emission at RT. Since the dipole–dipole transfer rate scales with donor oscillator strength, also the energy transfer rates are expected to be two orders of magnitude slower. The luminescence decay curves of QD films of 2.5 nm PbS QDs are shown in Fig. 19. The QDs in the film emit around 960 nm (920 nm in the solvent). The fast emission of the short wavelength side (donors) and the build-up on the long wavelength side (acceptors) indicate that the donor–acceptor transfer time for PbS QDs is about 200–400 ns, indeed also two orders of magnitude slower than observed for CdSe or CdTe QDs.

3.3 Energy transfer from quantum dots to dye molecules and metal nanoparticles. Energy transfer between QDs is interesting mainly from a fundamental point of view and has no immediate prospect for application. The main field of application of QDs is in the area of imaging in living organisms. QDs are perfect labels for bio-imaging due to the high stability, tunability of emission color, broad excitation range and narrow emission band [68–70]. Also in this field energy transfer processes play an important role, but now it involves not only energy transfer between QDs but also energy transfer to dye molecules and interaction with metal nanoparticles. In this last section some examples will be discussed where interaction between QDs and dye molecules or metal nanoparticles are used.

An elegant method to probe interaction between proteins (or other biomolecules) is to take advantage of the strong distance dependence of fluorescence (or Förster) resonance energy transfer (FRET). Energy transfer commonly proceeds through dipole–dipole interaction (both for fluorescent dyes and QDs) with the well-known R^{-6} distance dependence. By labelling two different biomolecules with fluorescent probes, energy transfer from the higher energy emitting probe (donor) to the probe emitting at a lower energy takes place, so that the information on the proximity of the two probes (typically within 10 nm) can be obtained. This technique is widely used with different types of dye molecules and is a very sensitive method to study receptor–ligand interactions or conformational changes of a biomolecule. For example, a conformational change where two areas of a protein form an active center can be probed by binding different chromophores that are capable of FRET on specific positions in the protein molecule that come together or apart. This process can be measured on a single molecule level and the dynamics of the folding and unfolding can be monitored. The application of the QDs instead of dye molecules in this type of studies offers the same advantages as mentioned above for the straightforward labelling of biomolecules with QDs for fluorescence imaging where especially the high stability of chromophore's emission is important [71–73]. For dye molecules, changes in the relative intensity of donor and acceptor emission is severely affected by quenching of donor and acceptor molecules which complicates the analysis of changes in the intensity due to FRET in closely linked donor–acceptor pairs.

A classic study showing the great potential of QDs in a quantitative analysis of protein binding is based on binding maltose binding proteins (MBP-zb) with an

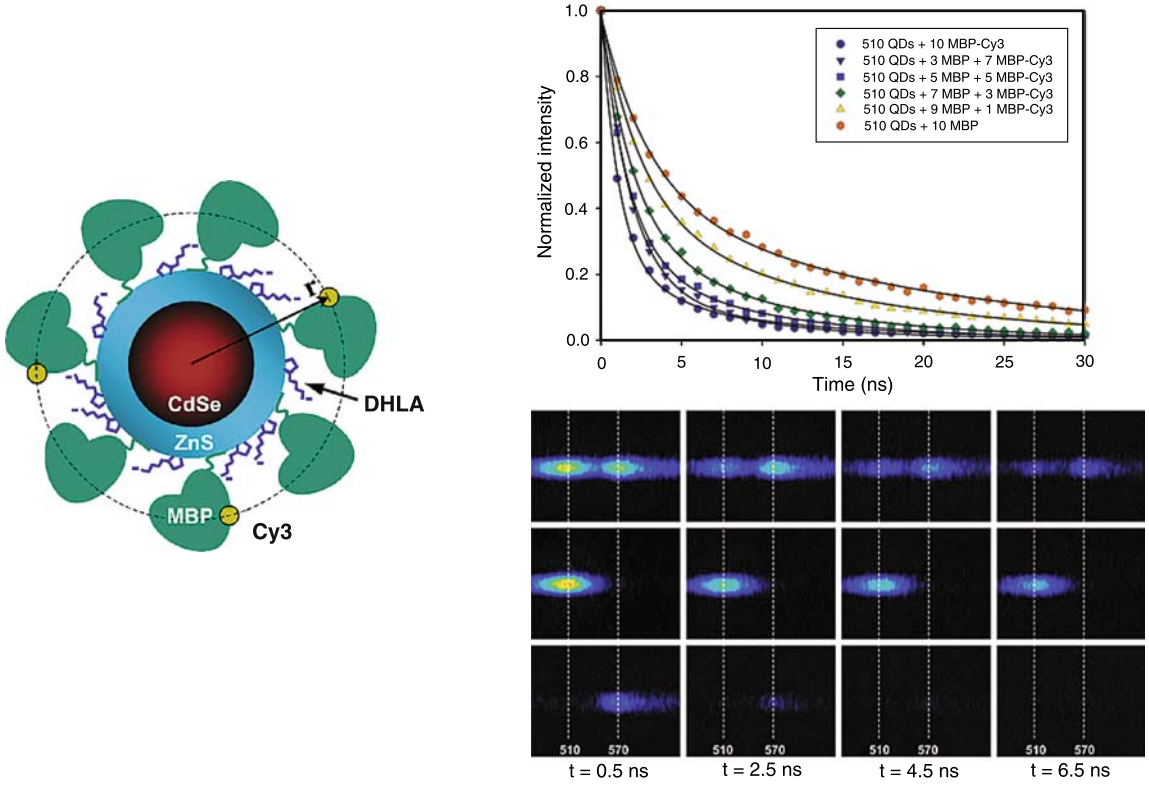

Fig. 20. (Left) Schematic representation of the QD–MBP-dye nanoassembly. The distance *r* represents the radius or average distance between the QD center and location of the Cy3-labeled residue on MBP. (Right) Plot of the 510 nm emitting QD photoemission intensity vs. time immediately after a short pulse excitation signal. Data are shown for various QD–MBP–Cy3 conjugate configurations where the number of Cy3-labeled proteins was increased from 0 to 10, while maintaining the total number of proteins fixed at 10 MBP/QD. Series of images showing the intensity of 510 nm QDs with 3 MBP/7 MBP-Cy3 (top row), 510 nm QDs with 10 MBP per QD (middle row), and free MBP-Cy3 equivalent to 10 MBP-Cy3 per QD (no QDs present, bottom row) as recorded by the CCD camera at 2 ns intervals. Reproduced with permission from [74], © 2004 ACS

electrostatic attachment domain irreversibly onto surfaces of CdSe/ZnS core shell QDs capped with dihydrolipoic acid ligands [74]. By attaching a cyanine dye (Cy3) to MPD dye-labeled proteins could be bound at a well-defined distance from the QD which acts as a donor due to the spectral overlap of the QD emission with the Cy3 absorption spectrum. The QD–MBP-dye complex is shown schematically in Fig. 20. Up to 15 MPD-proteins could be bound to the QD surface. By varying the number of MPD proteins with a dye molecule, the number of acceptors around the QD could be accurately varied (thus changing the acceptor concentration). Alternatively, the donor acceptor distance and the spectral overlap between the donor emission and the acceptor absorption could be varied by changing the size of the CdSe core. In Fig. 20 (right hand side) the QD decay curves are shown for different numbers of Cy3 acceptor, while in the images below the emission spectra recorded with a streak camera at different time intervals after the excitation pulse are shown. The decay curves show that the donor emission decay becomes progressively faster as the number of Cy3 acceptors around the QD donor increases. Analysis of the results allowed an accurate determination of the Förster distance for energy transfer ($\sim$6–7 nm) that was in excellent agreement (within 0.3 nm) with the distance determined using structural characterization techniques.

The control of energy transfer between asymmetric CdSe/CdS quantum rods (QRs) and dye molecules has been demonstrated at low temperatures and using an electric field [75]. At low temperatures the emission of the QRs becomes narrow, as do the absorption spectra of dye molecules. An important property of this particular kind of QRs is the much larger shift of the emission in an external electric field (as compared to QDs) [76]. This so-called quantum confined Stark effect (QCSE) in QRs was used to shift the emission of the QR in or out of resonance with the absorption spectrum of a nearby dye molecule (a Cy5 derivative). The QRs and dye molecules are incorporated (at well-chosen concentrations so that the distance between QRs and dye molecules is 20 nm on average) in a polystyrene film. The idea of the experiment is presented in Fig. 21, left hand side. Below the TEM-images showing the asymmetric CdSe/CDs QRs with a CdSe core located at one end of the nanostructure, the shift of the QR emission in resonance with the dye absorption upon applying an electric field is schematically depicted. On the right hand side of Fig. 21 it is demonstrated that the concept works beautifully: in the top graph the QR emission is shown for a film without dye molecules, demonstrating a 10 nm Stark shift upon cyclic application of a bias. In the lower images (b and c) turning on (b) and turning off (c) of Förster energy transfer by the electric field are shown. Depending on the resonance conditions for an individual QR-dye pair the electric field can shift the QR emission in or out of resonance with the dye absorption, thus electrically switching energy transfer.

Finally, energy transfer between QDs and metal nanoparticles is a hot topic. In spite of an exploding number of papers in this field (often called plasmonics), the basic understanding of the interactions that govern the response of excitons in QDs (or fundamental excitations in order systems) in the proximity of a metal nanoparticle is still lacking. In addition, the practical implications of plasmonic interactions seem to be only limited by ones imagination. To illustrate this, the influence of plasmonic coupling on the exciton life time is shown to be able to probe with a nm accuracy the

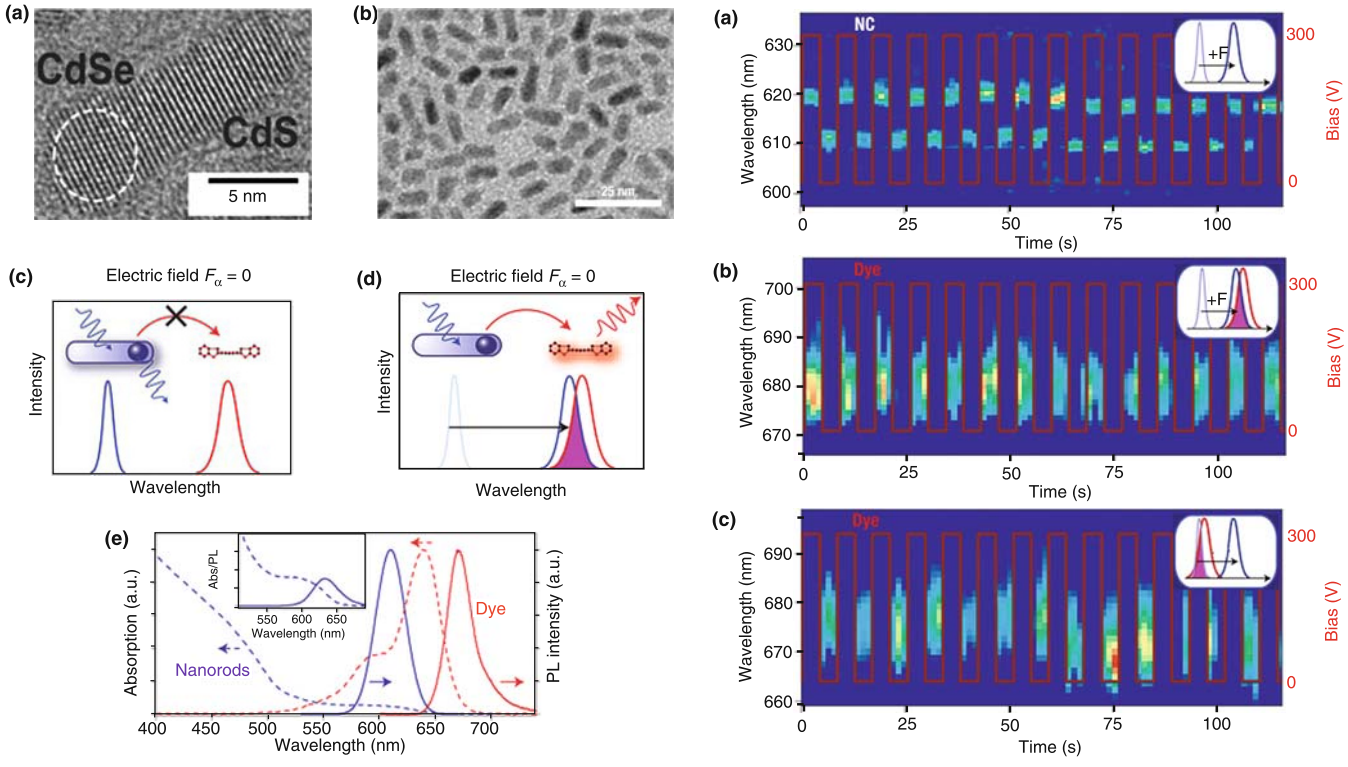

Fig. 21. (Left) **a**, **b** High-resolution TEM image and overview of CdSe/CdS quantum rods (QRs). **c**, **d** Schematic representation of spectral shifting the QR emission to overlap with the dye absorption by applying an electric field. **e** Ensemble excitation and emission spectra of the CdSe/CdS QRs and dye molecules at 50 K. (Right) Electrical tuning of resonant energy transfer from nanocrystals to single dye molecules using the QCSE at 50 K. **a** Dependence of the PL spectrum of a single nanocrystal on electric field in the absence of dye molecules. **b**, **c** Modulation of the fluorescence of two different nanocrystal–dye couples by cyclic application of a bias. Depending on the spectral position of the nanocrystal, FRET occurs either with (**b**) or without (**c**) an electric field, so that the dye emission switches on and off with a change in field. Reproduced with permission from [75], © 2006 Nature Publishing Group

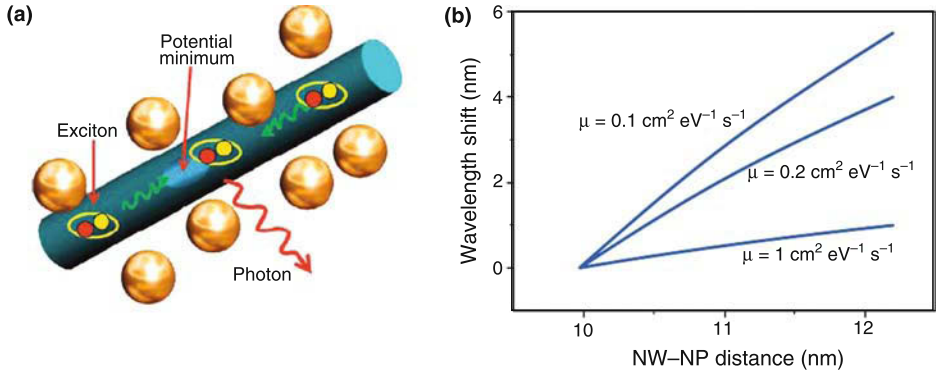

Fig. 22. **a** Schematic diagram of excitons diffusing towards the potential minima where they recombine. This leads to red-shifted emission. **b** Calculated wavelength shift of exciton emission as a function of the NW–NP distance for the specified exciton mobilities. Reproduced with permission from [77], © 2006 Nature Publishing Group

distance between a semiconductor nanowire (NW) and a gold nanoparticle [77]. This very sensitive distance probe can potentially be used in living cells to monitor the movement of biomolecules with nm accuracy. The basic idea is that the exciton life time in a semiconductor nanowire determines the emission wavelength. As the exciton diffuses in the nanowire it will be trapped in regions of lower bandgap separation and the longer the exciton lives, the larger the red-shift will be. The exciton life time will be shortened by energy transfer to a nearby metal nanoparticle and for simplicity the energy transfer rate is described by the Förster formula (giving a R^{-6} distance dependence). Based on these considerations the wavelength shifts to the blue as the metal nanoparticle approaches the wire (shortening the exciton life time) and shifts to the red as the metal nanoparticle moves away. The wavelength shift as a function of NW–NP is shown in Fig. 22 for different exciton mobilities.

To illustrate that this concept does indeed work, a molecular spring assembly was constructed as shown in Fig. 23 in which a CdTe nanowire is linked via PEG–aB–PEG strings to gold nanoparticles (PEG being poly-ethyleneglycol, aB being an antibody, here streptavidine SA, further details can be found in [77]). Upon adding an antigen (aG) that binds to the aB, the PEG chain expands and the NW–NP distance increases. As a result, the exciton lifetime increases due to slower energy transfer to the gold NPs and the emission shifts to the red. Upon adding free aB that competes with the aG bound on the PEG string, the aG is released from the string, the string contracts and the expected blue-shift is observed. This fully reversible wavelength shift demonstrates the viability of this approach. From the shift also the exciton mobility was estimated to be 0.1–0.2 $\mathrm{cm^2\,eV^{-1}\,s^{-1}}$.

Research on the influence of metal nanoparticles on the exciton dynamics in QDs is an area where new results have emerged in the past years [78–80] and some of the most promising new schemes for applications of (enhanced) QD fluorescence have been proposed by taking advantage of exciton–plasmon interaction. The near future will show which of these will actually work, but even if it is only a fraction it will be a successful avenue.

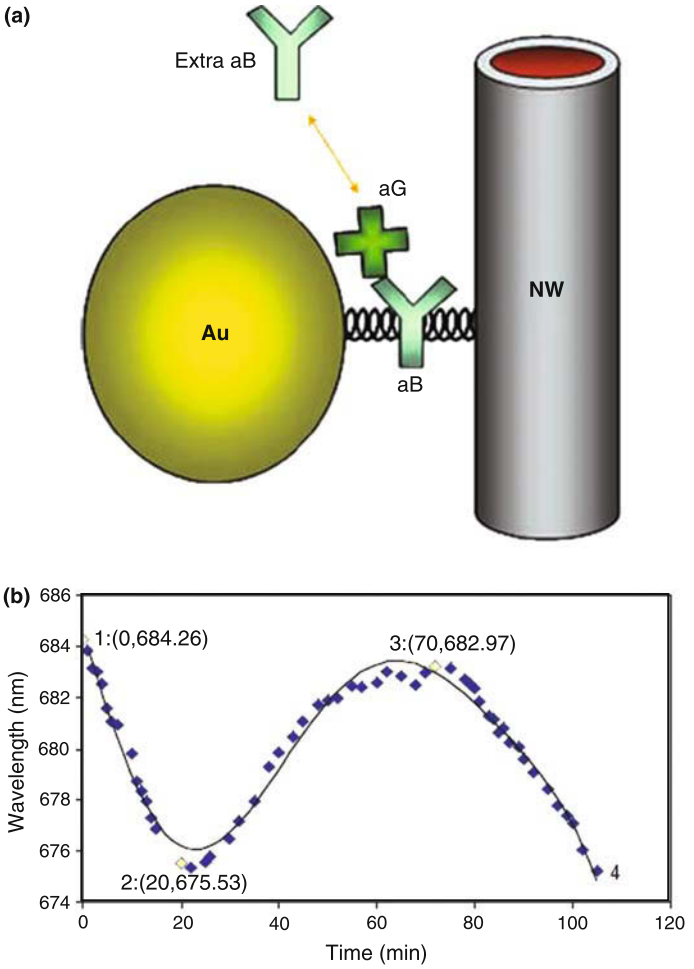

Fig. 23. a Schematic illustration of a molecular spring assembly of a CdTe nanowire linked via PEG–aB–PEG to a gold nanoparticle. The reversible coupling aG–aB (SA) changes the chain length. The addition of extra amounts of aB will disrupt the aG–aB reaction in the NP–PEG–aB–PEG–NW superstructure. **b** Reversible shift of the peak luminescence wavelength: 1, attachment of a NP to a NW; 2, after adding 20 µl SA; 3, after adding free aB to the media; 4, after adding 20 µl SA. Excitation wavelength: 420 nm. Reproduced with permission from [77], © 2006 Nature Publishing Group

4. Conclusions

Studies on the exciton dynamics in QDs have greatly contributed to the understanding of the energy level structure and dynamic processes in QDs in a broad time window (fs–ns). The research has benefited from the rapid development of generally accessible equipment for fast time resolved spectroscopy. Especially for the colloidal II–VI CdSe and CdTe QDs dynamic processes like exciton recombination, charge carrier relaxation and energy transfer are extensively studied and well understood. Nevertheless, these model systems will continue to be of great interest for the discovery of new phenomena. An important new focus in exciton dynamics studies is

aimed at controlling and understanding changes in the exciton dynamics through external influences, for example plasmonic coupling or embedding in photonic structures. For the infrared emitting IV–VI QDs PbSe and PbS a rising interest in the exciton dynamics has been triggered by potential application for telecommunication and reports on multiple exciton generation. Energy transfer processes involving QDs have been widely studied and can be well explained using the Förster theory for energy transfer. Exciting developments in this area involve controlling energy transfer on a nm scale where especially coupling with metal nanoparticles or dye molecules offer new avenues for detection schemes that can be used in bio-imaging and possibly other areas. In the past 10 years of research on exciton dynamics has developed into a mature and exciting field that continues to attract a growing number of (young) researchers.

References

[1] Jaeckel G (1926) Some modern absorption glasses. Z Tech Phys 7: 301–304
[2] Rossetti R, Nakahara S, Brus LE (1983) Quantum size effects in the redox potentials, resonance Raman spectra, and electronic spectra of cadmium sulfide crystallites in aqueous solution. Journal of Chemical Physics 79: 1086–1088
[3] Henglein A (1982) Photodegradation and fluorescence of colloidal cadmium sulfide in aqueous solution. Berichte der Bunsen-Gesellschaft Physikalische Chemie 86: 301–305
[4] Ekimov AI, Onushchenko AA (1981) Quantum dimensional effect in three-dimensional microcrystals of semiconductors. Pis'ma v Zhurnal Eksperimental'noi i Teoreticheskoi Fiziki 34: 363–366
[5] Henderson B, Imbusch GF (1989) Optical spectroscopy of solids. Oxford University Press
[6] Wehrenberg BL, Wang C, Guyot-Sionnest P (2002) Interband and intraband optical studies of PbSe colloidal quantum dots. Journal of Physical Chemistry B 106: 10634–10640
[7] Murray CB, Norris DJ, Bawendi M (1993) Synthesis and characterization of nearly monodisperse CdE (E = sulfur, selenium, tellurium) semiconductor nanocrystallites. Journal of the American Chemical Society 115: 8706–8715
[8] Nirmal M, Murray CB, Bawendi M (1994) Fluorescence-line narrowing in CdSe quantum dots: surface localization of the photogenerated exciton. Physical Review B: Condensed Matter 50: 2293–2300
[9] Efros AL, Rosen M, Kuno M, Nirmal M, Norris DJ, Bawendi M (1996) Band-edge exciton in quantum dots of semiconductors with a degenerate valence band: dark and bright exciton states. Physical Review B: Condensed Matter 54: 4843–4856
[10] Bryant GW, Jaskolski W (2003) Tight-binding theory of quantum – dot quantum wells: single-particle effects and near-band-edge structure. Physical Review B: Condensed Matter and Materials Physics 67(20): 205320
[11] Califano M, Franceschetti A, Zunger A (2005) Temperature dependence of excitonic radiative decay in CdSe quantum dots: the role of surface hole traps. Nano Letters 5: 2360–2364
[12] Leung K, Pokrant S, Waley KB (1998) Exciton fine structure in CdSe nanoclusters. Physical Review B 57: 12291–12301
[13] Mello Donegá de C, Bode M, Meijerink A (2006) Size- and temperature-dependence of exciton lifetimes in CdSe quantum dots. Physical Review B 74: 085320/1–085320/9
[14] Crooker SA, Barrick T, Hollingsworth JA, Klimov VI (2003) Multiple temperature regimes of radiative decay in CdSe nanocrystal quantum dots: intrinsic limits to the dark-exciton lifetime. Applied Physics Letters 82: 2793–2795
[15] Labeau O, Tamarat P, Lounis B (2003) Temperature dependence of the luminescence. Lifetime of single CdSe/ZnS quantum dots. Physical Review Letters 90: 257404
[16] Wuister SF, Houselt van A, de Mello Donegá C, Vanmaekelbergh D, Meijerink A (2004) Temperature antiquenching of the luminescence from capped CdSe quantum dots. Angewandte Chemie-International Edition 43: 3029–3033
[17] Wuister SF, Mello Donegá de C, Meijerink A (2004) Luminescence temperature antiquenching of water-soluble CdTe quantum dots: role of the solvent. Journal of the American Chemical Society 126: 10397–10402
[18] Qu L, Peng X (2002) Control of photoluminescence properties of CdSe nanocrystals in growth. Journal of the American Chemical Society 124: 2049–2055

[19] Reiss P, Carayon S, Bleuse J (2003) Large fluorescence quantum yield and low size dispersion from CdSe/ZnSe core/shell nanocrystals. Physica E: Low-Dimensional Systems & Nanostructures 17: 95–96
[20] Mello Donegá de C, Hickey SG, Wuister SF, Vanmaekelbergh D, Meijerink A (2003) Single-step synthesis to control the photoluminescence quantum yield and size dispersion of CdSe nanocrystals. Journal of Physical Chemistry B 107: 489–496
[21] Wuister SF, de Mello Donegá C, Meijerink A (2004) Influence of thiol capping on the exciton luminescence and decay kinetics of CdTe and CdSe quantum dots. Journal of Physical Chemistry B 108: 17393–17397
[22] Wuister SF, de Mello Donegá C, Meijerink A (2004) Local-field effects on the spontaneous emission rate of CdTe and CdSe quantum dots in dielectric media. Journal of Chemical Physics 121: 4310–4315
[23] Lodahl P, Driel van AF, Nikolaev IS, Irman A, Overgaag K, Vanmaekelbergh D, Vos WL (2004) Controlling the dynamics of spontaneous emission from quantum dots by photonic crystals. Nature 430: 654–657
[24] Driel van AF, Allan G, Delerue C, Lodahl P, Vos WL, Vanmaekelbergh D (2005) Frequency-dependent spontaneous emission rate from CdSe and CdTe nanocrystals: influence of dark states. Physical Review Letters 95: 236804/1–236804/4
[25] Nozik AJ (2001) Spectroscopy and hot electron relaxation dynamics in semiconductor quantum wells and quantum dots. Annual Reviews in Physical Chemistry 52: 193–231
[26] Guyot-Sionnest P, Wehrenberg B, Yu D (2005) Intraband relaxation in CdSe nanocrystals and the strong influence of the surface ligands. Journal of Chemical Physics 123: 074709
[27] Boudreaux DS, Williams F, Nozik AJ (1980) Hot carrier injection at semiconductor-electrolyte junctions. Journal of Applied Physics 51: 2158–2163
[28] Dijkhuis JI, Pol van der A, Wijn de HW (1976) Spectral width of optically generated bottlenecked ($29\,cm^{-1}$) phonons in ruby. Physical Review Letters 37: 1554–1557
[29] Tilstra LG, Arts AFM, Wijn de HW (2007) Optically excited ruby as a saser: experiment and theory. Physical Review B 76: 024302
[30] Heitz R, Born H, Guffarth F, Stier O, Schliwa A, Hoffmann A, Bimberg D (2001) Existence of a phonon bottleneck for excitons in quantum dots. Physical Review B: Condensed Matter and Materials Physics 64: 241305
[31] Kral K, Khas P (1998) Absence of phonon bottleneck and fast electronic relaxation in quantum dots. Physica Status Solidi B: Basic Research 208: R5–R6
[32] Guyot-Sionnest P, Shim M, Matranga C, Hines M (1999) Intraband relaxation in CdSe quantum dots. Physical Review B: Condensed Matter and Materials Physics 60: R2181–R2184
[33] Rufo S, Dutta M, Stroscio MA (2003) Acoustic modes in free and embedded quantum dots. Journal of Applied Physics 93: 2900–2905
[34] Klimov V (2000) Optical nonlinearities and ultrafast carrier dynamics in semiconductor nanocrystals. Journal of Physical Chemistry B 104: 6112–6123
[35] Wang H, Mello Donegá de C, Meijerink A, Glasbeek M (2006) Ultrafast exciton dynamics in CdSe quantum dots studied from bleaching recovery and fluorescence transients. Journal of Physical Chemistry B 110: 733–737
[36] Htoon H, Cox PJ, Klimov VI (2004) Structure of excited-state transitions of individual semiconductor nanocrystals probed by photoluminescence excitation spectroscopy. Physical Review Letters 93: 187402
[37] Salvador MR, Hines MA, Scholes GD (2003) Exciton-bath coupling and inhomogeneous broadening in the optical spectroscopy of semiconductor quantum dots. Journal of Chemical Physics 118: 9380–9388
[38] Caruge J-M, Chan Y, Sundar V, Eisler HJ, Bawendi MG (2004) Transient photoluminescence and simultaneous amplified spontaneous emission from multiexciton states in CdSe quantum dots. Physical Review B 70: 085316
[39] Fisher B, Caruge JM, Zehnder D, Bawendi M (2005) Room-temperature ordered photon emission from multiexciton states in single CdSe core-shell nanocrystals. Physical Review Letters 94: 087403
[40] Schaller RD, Klimov VI (2004) High efficiency carrier multiplication in PbSe nanocrystals: implications for solar energy conversion. Physical Review Letters 92: 186601
[41] Schaller RD, Sykora M, Pietryga JM, Klimov VI (2006) Seven excitons at a cost of one: redefining the limits for conversion efficiency of photons into charge carriers. Nano Letters 6: 424–429
[42] Warner JH, Thomsen E, Watt AR, Heckenberg NR, Rubinsztein-Dunlop H (2005) Time-resolved photoluminescence spectroscopy of ligand-capped PbS nanorystals. Nanotechnology 16: 175–179

[43] Clark SW, Harbold JM, Wise FW (2007) Resonant energy transfer in PbS quantum dots. Journal of Physical Chemistry C 111: 7302–7305
[44] An JM, Franceschetti A, Zunger A (2007) The excitonic exchange splitting and radiative life time in PbSe quantum dots. Nano Letters 7: 2129–2135
[45] Rijssel van J, Koole R, Mello Donegá de C, Meijerink A, unpublished
[46] Schaller RD, Petruska MA, Klimov VI (2005) The effect of electronic structure on carrier multiplication efficiency: a comparative study of PbSe and CdSe nanocrystals. Applied Physics Letters 87: 253102
[47] Pijpers JJH, Hendry E, Milder MTW, Fanciulli R, Savolainen J, Herek JL, Vanmaekelbergh D, Ruhman S, Mocatta D, Oron D, Aharoni A, Banin U, Bonn M (2007) Carrier multiplication and its reduction by photodoping in colloidal InAs quantum dots. Journal of Physical Chemistry C 111: 4146–4152
[48] Timmerman D, Izeddin I, Stallinga P, Yassievich IN, Gregorkiewicz T (2008) Space-separated quantum cutting with silicon nanocrystals for photovoltaic applications. Nature Photonics 2: 105–109
[49] Nair G, Bawendi MG (2007) Carrier multiplication yields of CdSe and CdTe nanocrystals by transient photoluminescence spectroscopy. Physical Review B 76: 081304(R)
[50] Itoh T, Iwabuchi Y, Ikehara T, Furumiya M, Katagiri N, Yano S, Iwai S, Edamatsu K, Gourdon C, Ekimov A (1999) Fundamental and nonlinear optical properties of semiconductor mesoscopic particles. Mesoscopic Materials and Clusters 31: 31–46
[51] Berstermann T, Auer T, Kurtze H, Schwab M, Yakovlev DR, Bayer M, Wiersig J, Gies C, Jahnke F, Reuter D, Wieck AD (2007) Systematic study of carrier correlations in the electron–hole recombination dynamics of quantum dots. Physical Review B: Condensed Matter and Materials Physics 76: 165318
[52] Lucey DW, MacRae DJ, Furis M, Sahoo Y, Cartwright AN, Prasad PN (2005) Monodispersed InP quantum dots prepared by colloidal chemistry in a noncoordinating solvent. Chemistry of Materials 17: 3754–3762
[53] Xiong G, Pal U, Serrano JG (2007) Correlations among size, defects, and photoluminescence in ZnO nanoparticles. Journal of Applied Physics 101: 024317
[54] Hirai T, Harada Y, Hashimoto S, Itoh T, Ohno N (2005) Luminescence of excitons in mesoscopic ZnO particles. Journal of Luminescence 112: 196–199
[55] Calcott PDJ (1998) The mechanism of light emission from porous silicon: where are we 7 years on? Materials Science & Engineering B: Solid-State Materials for Advanced Technology B51: 132–140
[56] Godefroo S, Hayne M, Jivanescu M, Stesmans A et al (2008) Classification and control of the origin of photoluminescence from Si nanocrystals. Nature Nanotechnology 3: 174–178
[57] Dovrat M, Goshen Y, Jedrzejewski J, Balberg I, Sa'ar A (2004) Radiative versus nonradiative decay processes in silicon nanocrystals probed by time-resolved photoluminescence spectroscopy. Physical Review B: Condensed Matter and Materials Physics 69: 155311
[58] Walters RJ, Kalkman J, Polman A, Atwater HA, de Dood MJA, Watson TJ (2006) Photoluminescence quantum efficiency of dense silicon nanocrystal ensembles in SiO_2. Physical Review B: Condensed Matter and Materials Physics 73: 132302
[59] Allan G, Delereu C (2007) Energy transfer between semiconductor nanocrystals: validity of Forster's theory. Physical Review B: Condensed Matter and Materials Physics 75: 195311
[60] Siebold H, Heber J (1981) "Discrete shell model" for analyzing time-resolved energy transfer in solids. Journal of Luminescence 22: 297–319
[61] Vergeer P, Vlugt TJH, Kox MHF, Hertog den MI, Eerden van der JPJM, Meijerink A (2005) Quantum cutting by cooperative energy transfer in $YbxY_{1-x}PO_4$: Tb^{3+}. Physical Review B 71: 014119
[62] Kagan CR, Murray CB, Nirmal M, Bawendi MG (1996) Electronic energy transfer in CdSe quantum dot solids. Physical Review Letters 76: 1517–1520
[63] Kagan CR, Murray CB, Bawendi MG (1996) Long-range resonance transfer of electronic excitations in close-packed CdSe quantum-dot solids. Physical Review B: Condensed Matter 54: 8633–8643
[64] Achermann M, Petruska MA, Crooker SA, Klimov VI (2003) Picosecond energy transfer in quantum dot Langmuir-Blodgett nanoassemblies. Journal of Physical Chemistry B 107: 13782–13787
[65] Franzl T, Koktysh DS, Klar TA, Rogach AL, Feldmann J, Gaponik N (2004) Fast energy transfer in layer-by-layer assembled CdTe nanocrystal bilayers. Applied Physics Letters 84: 2904–2906
[66] Crooker SA, Hollingsworth JA, Tretiak S, Klimov VI (2002) Spectrally resolved dynamics of energy transfer in quantum-dot assemblies: toward engineered energy flows in artificial materials. Physical Review Letters 89: 186802

[67] Wuister SF, Koole R, Mello Donegá de C, Meijerink A (2005) Temperature-dependent energy transfer in cadmium telluride quantum dot solids. Journal of Physical Chemistry B 109: 5504–5508
[68] Bruchez M, Moronne M, Gin P, Weiss S, Alivisatos P (1998) Semiconductor nanocrystals as fluorescent biological labels. Science 281: 2013–2016
[69] Chan WCW, Nie SM (1998) Quantum dot bioconjugates for ultrasensitive nonisotopic detection. Science 281: 2016–2018
[70] Alivisatos P (2004) The use of nanocrystals in biological detection. Nature Biotechnology 22: 47–52
[71] Willard DM, Carillo LL, Jung J, Van Orden A (2001) CdSe-ZnS quantum dots as resonance energy transfer donors in model protein-rotein binding assay. Nano Letters 1: 469–474
[72] Ebenstein Y, Mokari T, Banin U (2004) Quantum dot functionalized scanning probes for fluorescence-energy-transfer-based microscopy. Journal of Physical Chemistry B 108: 93–99
[73] Hohng S, Ha T (2005) Single-molecule quantum dot fluorescence resonance energy transfer. Chem Phys Chem 6: 956–960
[74] Clapp AR, Medintz IL, Mauro M, Fisher BR, Bawendi MG, Mattoussi H (2004) Fluorescence resonance energy transfer between quantum dot donors and dye-labeled protein acceptors. Journal of the American Chemical Society 126: 301–310
[75] Becker K, Lupton JM, Müller J, Rogach AL, Talapin DV, Weller H, Feldmann J (2006) Electrical control of Förster energy transfer. Nature Materials 5: 777–781
[76] Müller J, Lupton JM, Lagoudakis P, Koeppe R, Rogach AL, Feldmann J, Talapin D, Weller H (2005) Wave function engineering in elongated semiconductor nanocrystals with heterogeneous carrier confinement. Nano Letters 5: 2044–2049
[77] Lee J, Hernandez P, Lee J, Govorov AO, Kotov NA (2007) Exciton–plasmon interactions in molecular spring assemblies of nanowires and wavelength-based protein detection. Nature Materials 6: 291–295
[78] Nikoobakht B, Burda C, Braun M, Hun M, El-Sayed MA (2002) The quenching of CdSe quantum dot photoluminescence by gold nanoparticles in solution. Photochemistry and Photobiology 75: 591–597
[79] Fu A et al. (2004) Discrete nanoctructures of quantum dots/Au with DNA Journal of American Chemical Society 126: 10832–10833
[80] Shevchenko EV, Ringler M, Schwemer A, Talapin DV, Klar TA, Rogach AL, Feldmann J, Alivisatos P (2008) Self-assembled binary superlattices of CdSe and Au nanocrystals and their fluorescence properties. Journal of the American Chemical Society 130: 3274–3275